Article

Discovery of SK-575 as a Highly Potent and Efficacious Proteolysis Targeting Chimera (PROTAC) Degrader of PARP1 for Treating Cancers

Chao-Guo Cao, Jie Yang, Yong Chen, Pei-Ting Zhou, Ying-Wei Wang, Wu Du, Li-Feng Zhao, and Yuanwei Chen

J. Med. Chem., **Just Accepted Manuscript** • DOI: 10.1021/acs.jmedchem.0c00821 • Publication Date (Web): 14 Sep 2020

Discovery of SK-575 as a Highly Potent and Efficacious Proteolysis Targeting Chimera (PROTAC) Degrader of PARP1 for Treating Cancers

Chaoguo Cao,[†,∇] Jie Yang,[†,∇] Yong Chen,[†,∇] Peiting Zhou,[†] Yingwei Wang,[†] Wu Du,[§] Lifeng Zhao,*[,‡] and Yuanwei Chen*[,†,§]

[†]State Key Laboratory of Biotherapy, Collaborative Innovation Center of Biotherapy and Cancer Center, West China Hospital of Sichuan University, Chengdu, 610041, China

[‡]Sichuan Industrial Institute of Antibiotics, Chengdu University, Chengdu 610052, China

[§]Hinova Pharmaceuticals Inc, 4th Floor, Building RongYao A, No. 5, Keyuan South Road, Chengdu, 610041, China

ABSTRACT:

The nuclear protein poly(ADP-ribose) polymerase-1 (PARP1) has a well-established role in the signaling and repair of DNA, and is a validated therapeutic target for cancers and other human diseases. Here, we have designed, synthesized, and evaluated a series of small-molecule PARP1 degraders based on the proteolysis targeting chimera (PROTAC) concept. Our efforts have led to the discovery of highly potent PARP1 degraders, as exemplified by compound **18** (SK-575). SK-575 potently inhibits the growth of cancer cells bearing BRCA1/2 mutations and induces potent and specific degradation of PARP1 in various human cancer cells even at low picomolar concentrations. SK-575 achieves durable tumor growth

inhibition in mice when used as a single-agent or in combination with cytotoxic agents, such as temozolomide (TMZ) and cisplatin. These data demonstrate that SK-575 is a highly potent and efficacious PARP1 degrader.

INTRODUCTION

Poly(ADP-ribose) polymerase-1 (PARP1) is the most abundant and well-characterized member of poly(ADP-ribose) polymerase (PARP) family of enzymes.[1-3] As a DNA-dependent nuclear enzyme, PARP1 plays a pivotal role in the signaling and repair of DNA damage.[2] Following DNA damage caused by the cell's own metabolic, chemical poisons or ionizing radiation,[4] PARP1 is rapidly activated, then recognizes and binds to DNA single-strand breaks (SSBs), where it catalyzes the fracture of nicotinamide adenine dinucleotide (NAD^+) to ADP-ribose and nicotinamide, and then transfers the ADP-ribose units to synthesize poly(ADP-ribose) (PAR) chains either on itself or on several acceptor proteins.[5-7] These PAR chains with more negative charges and larger steric hindrance can make PARP1 dissociate from DNA fracture by reducing the affinity between PARP1 and DNA, and then guide DNA repair factors to combine with DNA gap to repair the damaged part.[2,8,9] This is the key process known as base excision repair (BRE) pathway for DNA repair.[2,5]

The PARP1 knockout cancer cells and animals exhibit a high degree of sensitivity to radiation or cytotoxic agents.[10,11] Initially, PARP1 inhibitors (PARPi) were developed as promising co-adjuvant components of standard chemo- and radiotherapy for tumor therapy.[12-14] Cancer cells bearing mutations in BRCA-1 or -2 are exquisitely sensitive to PARPi, which is called 'synthetic lethality'.[15-17] In this regard, many small-molecule PARPi, such as olaparib,[18] rucarparib,[19] niraparib,[20] and talazoparib,[21] have been developed in different stages of clinical trials.[22] For instance, olaparib as the first oral potent PARP1/2 inhibitor, have been approved for the treatment of BRCA-mutation cancer in the clinic, especially for ovarian and breast cancers.[23] However, there are still challenges in terms of PARPi usage that limit their therapeutic utility, including the acquisition of drug resistance, the low proportion of BRCA-1 or -2

mutations in cancer cells.[15] In addition to the inhibition of PARP1 enzyme activity, the mechanism of action of PARPi as antitumor agents is via PARP1 trapping.[24,25] In short, PARPi prevent PARP1 protein from dissociating from DNA breaks to form PARP1-PARPi-DNA complexes, which could block and damage DNA replication, and is therefore more toxic than merely unrepaired SSBs due to the inactivation of PARP1. Thus, PARPi can kill tumor cells and are also toxic to normal cells.[26] However, we are unable to assess the relative contribution of these two pathways (PARP1 catalytic inhibition and trapping) to PARP inhibitor mediated cytotoxicity.

Besides the role in cancer cells, the overactivation of PARP1 has been associated with several pathophysiological conditions, such as neurological diseases (e.g., stroke, neurodegeneration),[27,28] ischemia-reperfusion injury (e.g., myocardial infarction),[29] severe acute critical illness (e.g., shock, acute lung injury, acute liver failure)[28,30,31] and inflammatory diseases[32]. In these non-oncological diseases, the overstimulation of PARP1 with the catalytic activity results in the cellular depletion of NAD^+ and forces the activation of the salvage synthesis pathway. NAD^+ depletion leads to ATP depletion, resulting in cellular energetic deficit and cell necrotic death.[33] Moreover, the overactivation of PARP1 leads to the accumulation of free PAR polymers to reach the cytotoxic level, which induces mitochondria release of apoptosis-inducing factors rapidly, leading to cell death termed parthanatos.[34] Several kinds of PARPi have been proved to be effective in non-oncological indications. However, their usage is still cautious, mainly due to their PARP1 trapping activity and mechanism-independent cytotoxicity.[24,35] Consequently, developing a practical strategy, by blocking both the catalytic and scaffolding functions of PARP1 without causing PARP1 trapping, is urgent and meaningful for PARP1-related diseases.

Proteolysis targeting chimera (PROTAC) concept can be dated back to 2001.[36] PROTAC molecules

are heterobifunctional small molecule containing two ligands, which specifically bind to the target protein and E3 ubiquitin ligase, respectively, tethered together by a linker. These molecules are capable of driving the target proteins to E3 ubiquitin ligase, which results in the formation of the ternary complex and leads to ubiquitination of the target proteins and consequent proteasome-mediated degradation.[37] In the past decade, PROTAC strategy has gained great progress in inducing target protein degradation in vitro and in vivo, such as BET,[38-42] AR,[43] ER,[44] ALK,[45] and CDK9,[46-48] which are attributed to the discovery of several highly potent small-molecule ligands for E3 ubiquitin ligase. Several PARP1/2 degraders have been reported, including compound **1**,[49] **2** (iRucaparib-AP5),[50] **3** (iRucaparib-AP6),[50] and **4** (iVeliparib-AP6)[50] (Figure 1). Compound **1**, based on the niraparib derivative and nutlin-3 derivative, specifically induced the PARP1 cleavage and cell apoptosis in the MDA-MB-231 cells. In comparison, two of compounds, **2** and **3**, prepared by using different lengths of all polyethylene glycol (PEG) linkers, were reported as potent and efficacious PARP1 degraders with half-maximal degrading concentration (DC_{50}) of 36 nM and 82 nM in primary rat neonatal cardiomyocytes, respectively. However, these compounds could not completely degrade the intracellular PARP1 protein, and the remaining part can still play a part of catalytic role, thus limiting their therapeutic efficacy. Besides, compound **4** emerged as a potent PARP2 degrader, which was designed using veliparib as the PARP2 ligand and thalidomide as a cereblon (CRBN) ligand.

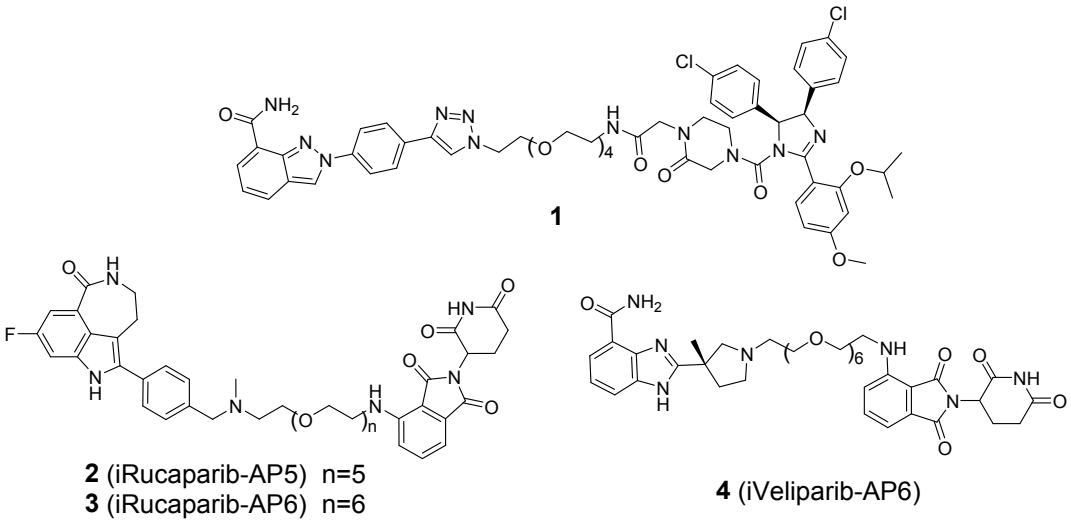

Figure 1. Chemical structure of three previously reported PARP1 degraders **1**, **2**, and **3**, and one previously reported PARP2 degraders **4**.

In this study, we describe the design, synthesis, and evaluation of PARP1-PROTAC degraders based upon a PAPR1 inhibitor olaparib and thalidomide/lenalidomide as ligands for cereblon/Cullin 4A. Our study has resulted in the discovery of highly potent PARP1-PROTAC degraders (hereafter called PARP1 degraders), exemplified by compound **18** (SK-575). SK-575 is capable of effectively inducing PARP1 protein degradation with the DC_{50} at the scale of picomolar (pM) and maximum degradation (D_{max}) > 95% in PARP1-positive cancer cell lines, and achieving durable tumor growth inhibition in mice at well-tolerated dose schedules. SK-575 is a highly potent and specific PARP1 degrader and warrants extensive evaluation for the treatment of cancers and other diseases.

RESULTS AND DISCUSSION

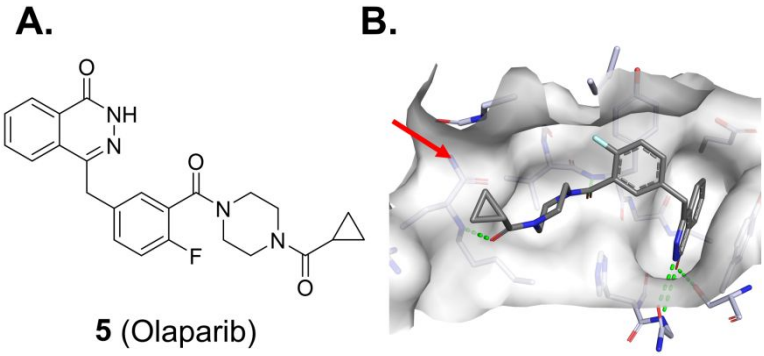

Figure 2. Design of PROTACs for PARP1. (A) Chemical structures of PARP1/2 inhibitor **5** (olaparib). (B) Crystal structure of **5** bound to the PARP1 catalytic domain (PDB ID: 5DS3). The possible linker tethering positions are shown in red arrows.

Design of PARP1 PROTAC Based on Olaparib. To explore the potential PARP1 degraders, we chose olaparib as the PARP1 ligand in our design for its excellent activity against PARP1/2 (Figure 2A).[18] According to the cocrystal structure of olaparib in the complex with PARP1 (Figure 2B), the amide moiety on olaparib is essential for binding to PARP1.[51] The cyclopropyl ring locates close to the opening of the ligand-binding pocket and thus may represent a suitable position to link with CRBN ligands without losing binding affinity dramatically. Based on the above design principles, we designed and synthesized a series of PARP1 targeting PROTACs using olaparib as the PARP1 ligand, diverse linkers, and thalidomide/lenalidomide as the CRBN ligands.

Determination of the Optimal Linker Length and Composition. It has been confirmed that a series of PARP1 degraders that conjugate olaparib to thalidomide with PEG unit fails to induce PARP1 degradation (see in Figure S1 in Supporting information).[49,50] We speculated that the length and the composition of the linker may be underexplored, and an optimized linker may induce favorable interaction between PARP1 and CRBN E3 ligase. Thus we have performed extensive optimization of the chemical

composition of the linker with different lengths. A series of PARP1 degraders, compounds **6-11** (Table 1), with different amino acid (e.g., using 4-aminobutyric acid and/or 6-aminocaproic acid) linkers were synthesized by a condensation reaction. Their growth inhibitory effect against BRCA1-deficient MDA-MB-436 and BRCA2-deficient Capan-1 cell lines, and the IC_{50} values (half-maximal growth inhibitory concentration) were then evaluated in a cell growth assay. Compound **11** has IC_{50} values of 0.95 μM in MDA-MB-436 and 1.5 μM in Capan-1, which were 52 and 56 times less potent than olaparib with IC_{50} values of 18 nM and 56 nM in these two cell lines, respectively. Next, changing the NH group in **10** to oxygen atom yielded **12** (Table 1), which showed IC_{50} values of 2.2 μM in MDA-MB-436 and 7.1 μM in Capan-1, and is less potent than **10**. The similar conversion of the NH group in **11** to an oxygen atom generated **13**, which has IC_{50} values of 1.7 μM and 2.2 μM in the inhibition of cell growth in MDA-MB-436 and Capan-1 cells, respectively, and is less potent than **11**. These results demonstrate that the amino acid linkers have an adverse influence on the cellular potency of the resulting PROTAC molecules. Thus, we identified that PROTAC molecules conjugating olaparib and CRBN ligand with amino acid linkers could not benefit for protein-protein interactions (PPIs) between CRBN E3 ligase and PARP1, cell penetration, and so on.

We next sought to investigate the optimal linkers and synthesized compounds **14-16**, **18**, and **20** that incorporated alkyl dicarboxylic acid of different lengths and ethylenediamine (Table 1). Surprisingly, compound **18**, which contained dodecarboxylic acid, displayed similar potency to olaparib in the cell growth inhibition, achieved IC_{50} values of 19 nM in MDA-MB-436 cells, and 56 nM in Capan-1 cells. Furthermore, changing the linker in **18** by decreasing or increasing one additional methylene group resulted in **17** or **19**, respectively, which are less potent than **18** in MDA-MB-436 and Capan-1 cells.

Table 1. Optimization of Linker Length and Composition of PARP1 Degraders

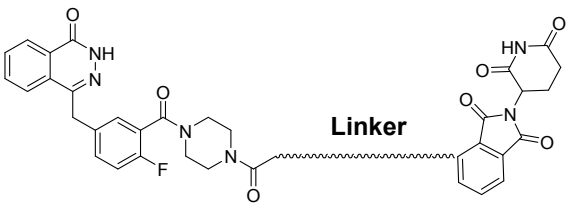

Compound	Linker	IC_{50} (μM) in cell growth inhibition[a]	
		MDA-MB-436	Capan-1
olaparib	-	0.018 ± 0.003	0.027 ± 0.005
6	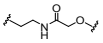	> 10	> 10
7	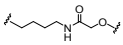	9.4 ± 3.1	> 10
8	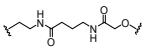	5.3 ± 1.9	> 10
9	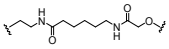	1.9 ± 1.1	8.7 ± 2.9
10	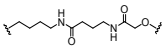	1.2 ± 0.7	3.1 ± 1.2
11	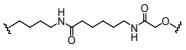	0.95 ± 0.22	1.5 ± 0.4
12	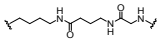	2.2 ± 1.3	7.1 ± 2.7
13	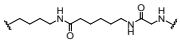	1.7 ± 0.7	2.2 ± 0.9
14	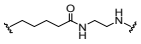	> 10	> 10
15	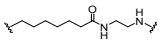	0.83 ± 0.26	4.1 ± 1.8
16	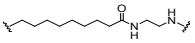	0.123 ± 0.071	0.495 ± 0.089
17	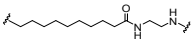	0.029 ± 0.008	0.264 ± 0.046
18 (SK-575)	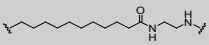	0.019 ± 0.006	0.056 ± 0.012
19	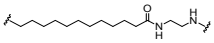	0.021 ± 0.003	0.087 ± 0.019
20	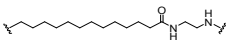	0.025 ± 0.004	0.118 ± 0.021

[a]IC_{50} values were obtained from three independent experiments (Mean ± SD).

Encouraged by the high potency of compound **18** in the inhibition of cell growth, we next synthesized

compounds **21** and **22** converting the -NH(CH$_2$)$_2$NH- group in **18** to a -NH(CH$_2$)$_4$NH- or -NH(CH$_2$)$_6$NH- group to further improve potency (Table 2). Compounds **21** and **22**, however, which were ~2 times less potent than compound **18** in cell growth inhibition, achieved IC$_{50}$ values of 39 nM and 42 nM in MDA-MB-436 cells, and 131 nM and 110 nM in Capan-1 cells, respectively. Furthermore, considering the linker length and chemical composition were important for PARP1 degraders to effectively inhibit cell growth, we replaced the -NH(CH$_2$)$_2$NH- group in **18** with a different length linker contained oxygen atom, and generated compounds **23-25** (Table 2). These compounds turned out to be less potent than compound **18** in cell growth inhibition. Consequently, these data thus established that a linker length of 15-16 atoms, as in compound **18** or **19**, is optimal for these PAPR1 degraders for inhibition of cell growth.

Table 2. Further Optimization of Linker Length and Composition

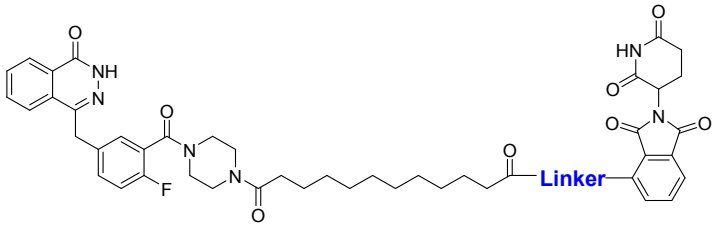

Compound	Linker	IC$_{50}$ (nM) in cell growth inhibition[a]	
		MDA-MB-436	Capan-1
18 (SK-575)		19 ± 6	56 ± 12
21		39 ± 12	131 ± 34
22	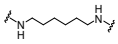	42 ± 12	110 ± 13
23	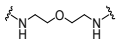	47 ± 18	120 ± 19
24	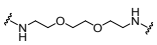	64 ± 21	134 ± 27
25	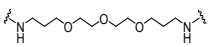	65 ± 23	154 ± 39

[a]IC$_{50}$ values were obtained from three independent experiments (Mean ± SD).

We further investigated the protein degradation activity of the resulting PARP1 degraders with an IC_{50} < 200 nM in MDA-MD-436 cells, and the protein level of PARP1 was analyzed through western blotting assay at four concentrations (1000, 100, 10 and 1 nM) in MDA-MB-436 and Capan-1 cell lines with 24 h treatment. As shown in Figure 3, compound **18** showed the best degradation activity at four concentrations in these two cancer cell lines, which is consistent with its cell growth inhibitory activity. In comparison, the corresponding PARP1 inhibitor, olaparib, fails to reduce the protein level of PARP1 at all concentrations tested (1-1000 nM). Compounds **20** and **21** with the same length linker have similar IC_{50} values in inhibition of cell growth, but they reveal different degradation activities. It may be that changes the position of the amide bond in linker influences the formation of special conformations. It is noteworthy that compound **21** effectively reduces the PARP1 protein by 70% at 10 nM and by 90.5% at 100 nM in MDA-MB-436 cell lines. Interestingly, compound **21** reduces PARP1 protein by 45% at 1 μM, less than that at 100 nM, probably due to the "hook" effect that has been observed previously for PROTAC degraders.[43,44,52]

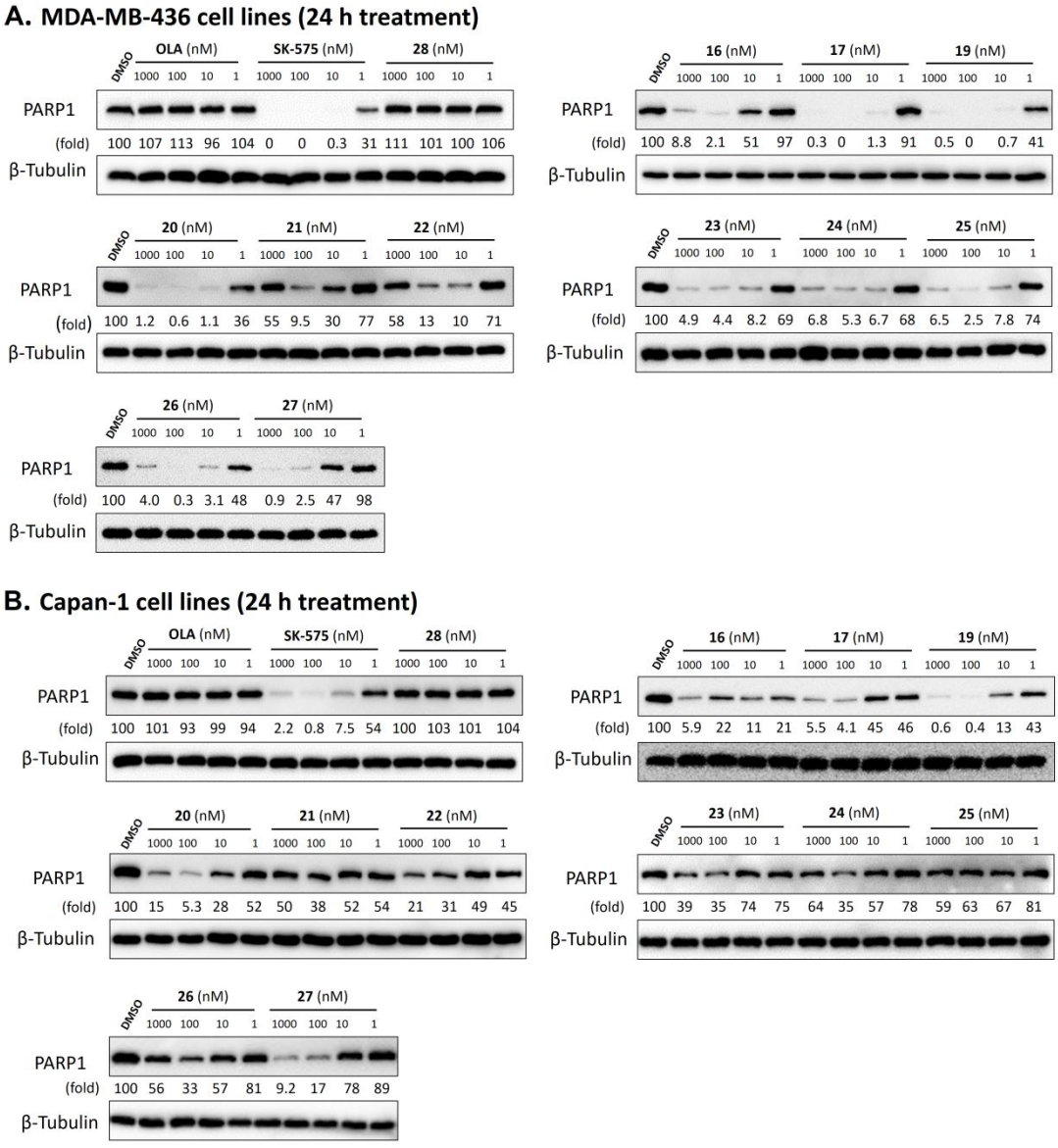

Figure 3. Western blotting analysis of PARP1 protein in MDA-MB-436 (A) and Capan-1 (B) cells treated with PARP1 inhibitor OLA (olaparib), PARP1 degraders **16-27**, and a control compound **28**. Cells were treated with each compound at 1, 10, 100, and 1000 nM for 24 h, and β-Tubulin was used as the loading control. The fold under the strip represents the PARP1/β-Tubulin ratio normalized with the DMSO control at 100.

Examination of the CRBN Ligand Portion in Compound 18. On the basis of **18**, we designed and synthesized compound **26** (Table 3) that tethered the phenyl ring of thalidomide from different positions.[53]

Compound **26** has IC_{50} values of 35 nM and 159 nM in inhibition of cell growth in MDA-MB-436 and Capan-1 cell lines, respectively, which is 2-3 times less potent than **18**. In addition, converting the 3-carbonyl group of thalidomide moiety in **18** to a methylene group generated **27**, which inhibits cell growth in MDA-MB-436 and Capan-1 cells with IC_{50} values of 92 nM and 194 nM, respectively, is 4-5 times less potent than compound **18**. Our western blotting analysis showed that **26** and **27** effectively induced PARP1 degradation, but their activities were weaker than **18** in these two cell lines mentioned above.

Table 3. Further Optimization of CRBN Ligand Portion in Compound 18

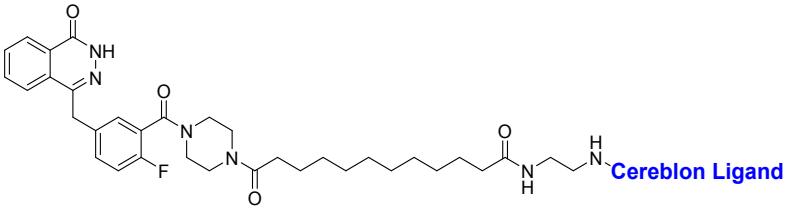

Compound	Cereblon Ligand	IC_{50} (nM) in cell growth inhibition[a]	
		MDA-MB-436	Capan-1
18 (SK-575)	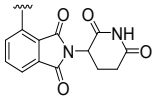	19 ± 6	56 ± 12
26	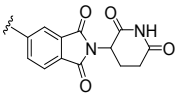	35 ± 15	159 ± 35
27	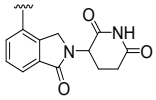	92 ± 23	194 ± 31

[a]IC_{50} values were obtained from three independent experiments (Mean ± SD).

Design and Synthesis of a Control Compound for 18. Revealing by the cocrystal structures, the amino group of the piperidine-2,6-dione in thalidomide forms a strong hydrogen bond with CRBN,[54,55] and methylation of the amino group of the piperidine-2,6-dione in thalidomide completely abrogates the

binding to CRBN.[42] We, therefore, synthesized compound **28** by methylation of the amino group of the piperidine-2,6-dione in compound **18** as an additional control compound (Figure 4). Compound **28** is completely ineffective in inducing PARP1 degradation in MDA-MB-436 and Capan-1 cells at concentrations up to 1 μM (Figure 3). These data clearly suggest that the induced degradation of PARP1 by compound **18** is cereblon/cullin-4A ligase-dependent, consistent with the PROTAC design.

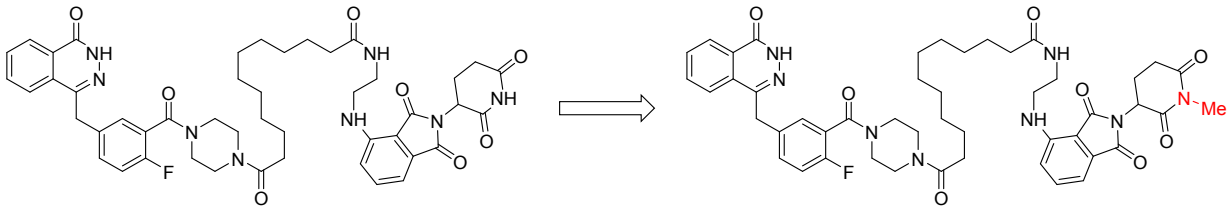

Figure 4. Design of **28** as a control compound.

Examination of the VHL Ligand Portion in Compound 18. Like CRBN ligands (such as thalidomide and its analogues), VHL ligands have been successfully used for the design of PROTAC degraders.[39,41, 43-44] Therefore, on the basis of **18**, we designed and synthesized compounds **29-32** using a VHL ligands (Table 4). Compound **29** has IC_{50} values of 54 nM and 87 nM in inhibition of cell growth in MDA-MB-436 and Capan-1 cell lines, respectively, which were 2-3 times less potent than **18**. After changing the linker length, the cell proliferation inhibitory activity of these compounds decreased when compared with **29**. Our western blotting analysis showed that compounds **29-32** have only a modest effect in reducing the level of PARP1 protein at 1 μM concentrations in the MDA-MB-436 cell lines (Figure S2). Taken together, these data indicated that these compounds mainly work as inhibitors, especially compound **29**, but not as PARP1 degraders. More studies are needed to determine if the VHL/cullin 2 E3 ligase system can be used for the design of highly potent and effective PARP1 degraders.

Table 4. Further Optimization of VHL Ligand Portion in Compound 18

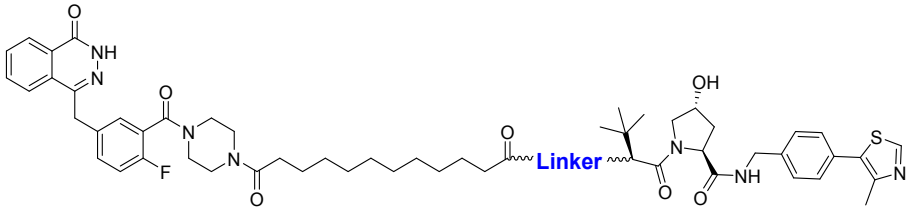

Compound	Linker	IC_{50} (μM) in cell growth inhibition[a]	
		MDA-MB-436	Capan-1
18 (SK-575)	-	0.019 ± 0.006	0.056 ± 0.012
29		0.054 ± 0.011	0.087 ± 0.023
30		1.2 ± 0.34	1.6 ± 0.39
32	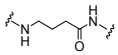	0.68 ± 0.11	0.87 ± 0.13
32	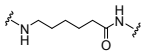	0.12 ± 0.021	0.17 ± 0.033
3 (iRucaparib-AP6)	-	0.71 ± 0.12	0.95 ± 0.22

[a]IC_{50} values were obtained from three independent experiments (Mean ± SD).

In direct comparison, the previously reported PARP1 degrader, compound **3** (iRucaparib-AP6), has IC_{50} values of 0.71 μM and 0.95 μM in inhibition of cell growth in MDA-MB-436 and Capan-1 cell lines, respectively, which are 36 and 17 times less potent than **18** (Table 4). Western blotting data showed that compound **18** are highly potent and effective in reducing PARP1 protein at 0.01-10 μM with a 12 h treatment in MDA-MB-436 and SW620 cell lines (Figure 5). However, compound **3** exhibited only modest effect in reducing the level of PARP1 protein at the same conditions.

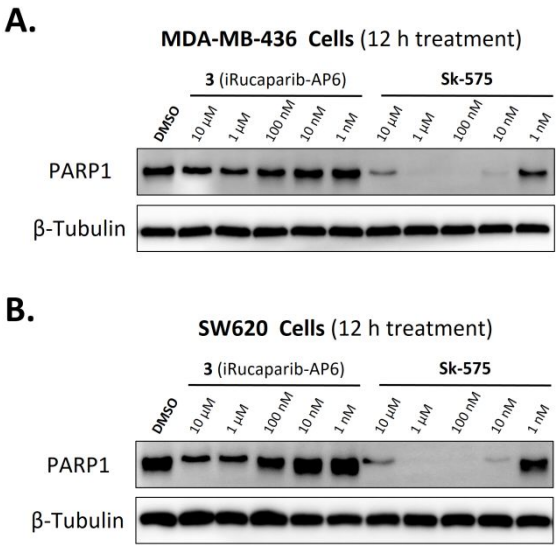

Figure 5. Western blotting analysis of PARP1 protein in MDA-MB-436 (A) and SW620 (B) cells treated with compounds **3** and **18**. Cells were treated with each compound at 1, 10, 100, 1000 nM, and 10 μM for 12 h, and β-Tubulin was used as the loading control.

Although compound **18** effectively induces degradation of the PARP1 protein at concentrations as low as 1-10 nM with 24 h treatment in MDA-MB-436 and Capan-1 cell lines, it has little or no effect on inducing degradation of the PARP2 protein in these two cell lines at concentrations up to 1 μM (Figure S3). Similarly, olaparib and compound **28** have no effect on the level of PARP2 protein. Hence, our data demonstrate that compound **18** is an efficient and specific PARP1 degrader. Based on the data of cell growth inhibition activity and degradation activity of PARP1, compound **18** appears to be the most potent PARP1 degrader among these resulting compounds. Consequently, we pursued an extensive investigation of compound **18** (SK-575).

Evaluation of Degradation Activity of SK-575 in Cancer Cells. We further evaluated SK-575 in MDA-MB-436, Capan-1, and SW620 cells for its potency in inducing PARP1 protein degradation with a 24 h treatment time in a wide range of concentrations (Figure 6A and S4). Quantification of our western

blotting data showed that SK-575 achieves DC_{50} values of 1.26 nM and 0.509 nM in the MDA-MB-436 and SW620 cells, respectively, and > 99% PARP1 degradation at 10 nM in these cell lines. SK-575, with a DC_{50} value of 6.72 nM, achieves near-complete degradation at 100 nM in Capan-1 cells.

We next evaluated the kinetics of SK-575 in the induction of PARP1 degradation at 30 nM in MDA-MB-436 and SW620 cell lines. Our data showed that SK-575 effectively reduces the PARP1 protein level within 1 h and achieves near-complete PARP1 depletion at the 2 h time-point, indicating fast kinetics (Figure 6B). The degradation activity of SK-575 in Capan-1 cell lines is weaker than that in MDA-MB-436 and SW620 cell lines, and it can reach the maximum degradation in 6 h at 100 nM.

To assess the durability of PARP1 protein degradation, we treated MDA-MB-436 cells with SK-575 at 100 nM for 5 days, illustrating that it induced sustained depletion of PARP1(Figure 6C). In another experiment, we treated MDA-MB-436 cells with SK-575 for 2 h at 100 nM and collected cells at various time points after compound washout. Our data showed that the level of PARP1 protein degrader-treated cells remained below the level in vehicle-treated cells, even 24 h after washout (Figure 6D).

To further assess the efficiency and broad applicability of SK-575, six different cancer cell lines were used to evaluate its potency in inducing PARP1 protein degradation with a 24 h treatment time. Surprisingly, besides the LNCaP cells achieved DC_{50} value at the nanomolar level (DC_{50} = 1.08 nM), the DC_{50} of all the tested cells were at the scale of picomolar after 24 h treatment (Figure 8A and Figure S4 in Supporting Information). The DC_{50} showed 384 pM in HCC1937, 512 pM in 22Rv1, 263 pM in MDA-MB-468, 578 pM in PC-3, and 228 pM in MDA-MB-231. It is noteworthy that SK-575 can reduce the PARP1 protein level by > 99% with a 24 h treatment time. At the same time, we also observed the rapid degradation of PARP1 protein in all of these cells (Figure S5 in Supporting Information). Taken together,

our data demonstrated that SK-575 not only displays the fast and efficient degradation of PARP1 but also has a broad application.

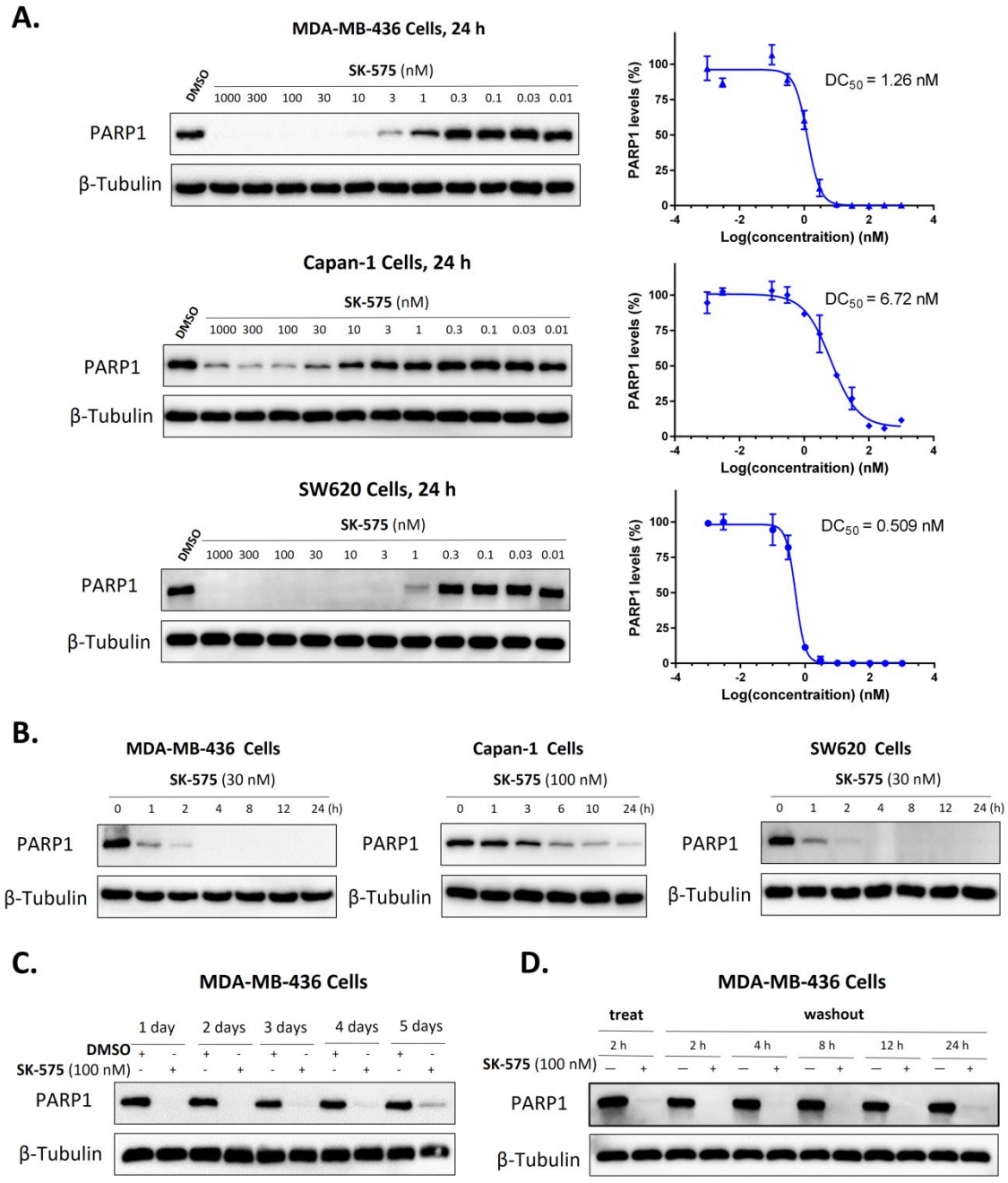

Figure 6. Further characterization of SK-575. (A) PARP1 degradation at the indicated dose of SK-575 with a 24 h treatment time in MDA-MB-436, Capan-1, and SW620 cells (left). PARP1 protein was examined by western blotting, and the PARP1 protein level was quantified and normalized to the corresponding density of β-Tubulin protein (right).

DC_{50} are calculated by two biologically independent experiments. (B) Time course of PARP1 degradation by SK-575 in MDA-MB-436 (30 nM), Capan-1 (100 nM), and SW620 (30 nM) cells. (C) Time course of PARP1 degradation by SK-575 in MDA-MB-436 (100 nM) cells. (D) Cellular PARP1 recovery levels after the washout of SK-575. Cells were pre-treated with SK-575 for 2 h and washout the compound for the indicated times.

Study on the Mechanism of SK-575. We investigated the mechanism of PARP1 degradation induced by SK-575 in MDA-MB-436 and SW620 cell lines, obtaining the results shown in Figure 7. The data showed that the degradation of PARP1 protein induced by SK-575 could be effectively blocked by pretreatment with a PARP1 inhibitor (olaparib) or a CRBN ligand (pomalidomide), in a dose-dependent manner for 24 treatment. These results supported that the high potency of SK-575 as a PARP1 degrader is dependent on binding to PARP1 and CRBN. Furthermore, a combination of proteasome inhibitor (MG132 or carfilzomib) or a NEDD8-activating enzyme (NAE) inhibitor (MLN4924) and SK-575 treatment completely blocked PARP1 degradation induced by SK-575, indicating that the fast and efficient PARP1 protein degradation by SK-575 was based on a NAE-mediated and proteasome-dependent mechanism. Taken together, these mechanistic data provided clear evidence that SK-575 is a bona fide PROTAC PARP1 degrader.

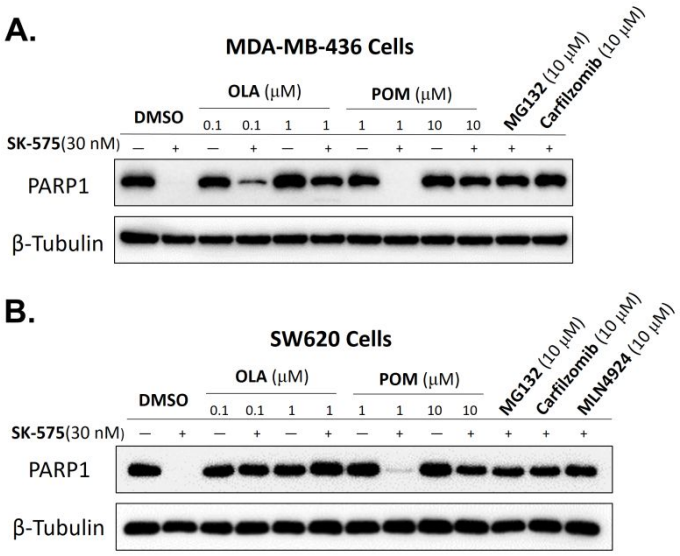

Figure 7. Western blotting analysis of PARP1 protein in MDA-MB-436 (A) and SW620 (B) cells after a 2 h pretreatment with PARP1 inhibitor OLA (olaparib), CRBN ligand POM (pomalidomide), proteasome inhibitor (MG132 or carfilzomib) or NEDD8-activating E1 enzyme inhibitor (MLN4924). Cells were treated with individual compound at indicated concentrations, following by a 24 h treatment with SK-575 at 30 nM, and β-Tubulin was used as the loading control.

Evaluation Activity of SK-575 in vitro. Using a PARP1 activity assay, we confirmed that SK-575 and its methylation counterpart **28** still strongly bound to PARP1, with IC_{50} values of 2.30 nM and 2.64 nM, respectively, which are equivalent to their parental inhibitor olaparib with an IC_{50} value of 3.35 nM (Figure 8B). Next, we further examined the ability of SK-575 and olaparib to suppress cell growth inhibitory of HR-deficient cell lines containing BRCA1/2 or PTEN, and HR-proficient cancer cell lines (Figure 8C and Table S1 in Supporting Information).[21,56] Both SK-575 and olaparib potently inhibit HR-deficient and HR-proficient cell growth with IC_{50} values at the micromolar level. However, SK-575 is more potent than olaparib， indicating that the potency of cell growth inhibition is due in part to their

ability to degrade PARP1. In addition, we evaluated the ability to potentiate the cytotoxic effect of SK-575 by alkylating agent methyl methanesulphonate (MMS). After a growth-inhibition curve for SW620 cells was established, the effectiveness of MMS was potentiated in a dose-dependent manner by adding PARP1 degrader at the concentration of nanomolar (Figure 8D). Moreover, we evaluated the preliminary safety of SK-575 with six normal cell lines (L-O2, HEK-293, NCM460, HUV-EC, MCF-10A, and H9c2), and the results were shown in Figure S6. Our data showed that the toxicity of SK-575 to these cells is acceptable, similar to olaparib.

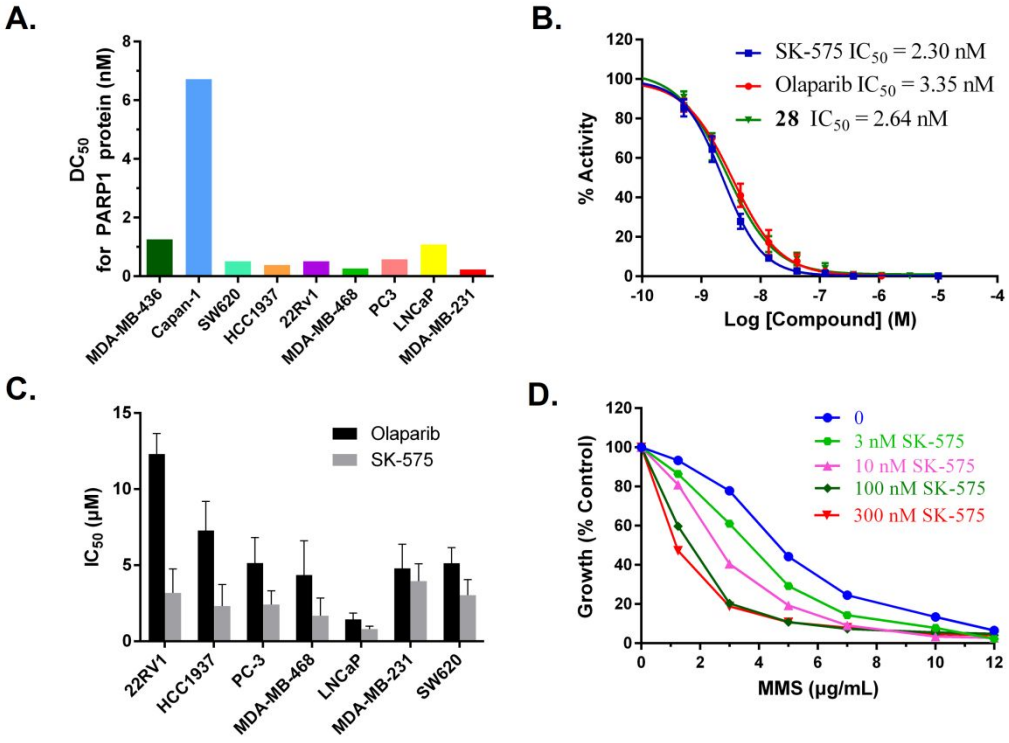

Figure 8. The highly potent and broad applicability of SK-575. (A) DC_{50} of SK-575 for PARP1 in different cancer cells. Data are the average of two biologically independent experiments. (B) PARP1 activity assay. (C) The IC_{50} valves of SK-575 and olaparib. Cells were treated with indicated doses for 7 days. Cell viability was determined by CCK-8 assay, and the data were calculated using the GraphPad Prism 7 software. (D) Potentiation of MMS cell killing of cultured SW620 cells in combination with SK-575. Increasing concentrations of MMS were co-incubated with or without the PARP1

degrader at single concentrations ranging from 3 to 300 nM.

Because DNA double-strand breaks (DSBs) induce the phosphorylation of histone H2AX (γH2AX) in the chromatin flanking the break site, the DNA damage levels can be monitored by estimating the formation of γH2AX.[57] We evaluated the ability of SK-575 and olaparib to induce the formation of γH2AX foci in the MDA-MB-436 (BRCA1$^{-/-}$) and Capan-1 (BRCA2$^{-/-}$) cell lines by western blotting assay. We found that SK-575 effectively induced the formation of γH2AX in these two cells in a dose-dependent manner. In contrast, olaparib exhibited a weaker ability than SK-575 at the same concentration (Figure 9).

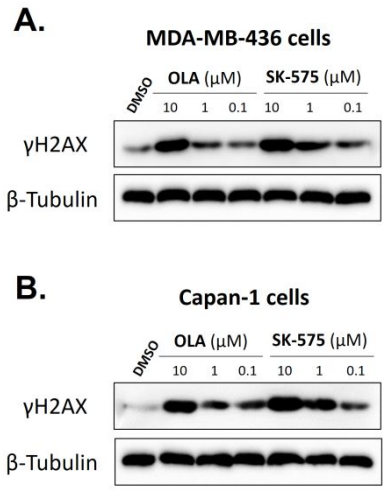

Figure 9. Western blotting analysis of γH2AX proteins in MDA-MB-436 (A) and Capan-1 (B) cells, with β-Tubulin used as the loading control. Cells were treated with PARP1 inhibitor (olaparib) or PARP1 degrader (SK-575) at indicated concentrations, following by a 24 h treatment.

Pharmacokinetics Evaluation of SK-575 in Mice. To assess the antitumor activity of SK-575 in vivo, we first performed a pharmacokinetics (PK) analysis in mice, and obtained the data shown in Figure 10A.

In this experiment, a single dose of SK-575 at 25 mg/kg intraperitoneally followed by plasma level quantitation revealed a maximum concentration of over 2.1 μM at 0.25 h postinjection, indicating that SK-575 is absorbed rapidly. In addition, our data showed that SK-575 with a half-life of 3.08 h (n = 3) has a concentration of 1.83 μM, 182 nM, and 95 nM in plasma at 1, 4, 8 h time-points, respectively. Importantly, the plasma concentration remains above 10 nM, a concentration needed for effective PARP1 degradation shown in our in vitro experiments, for 24 h postinjection. Taken together, our PK data indicate that a single dose of SK-575 at 25 mg/kg achieves a sufficient exposure in plasma for over 24 h.

Pharmacodynamics Evaluation of SK-575 in SW620 Xenograft Tumor Tissues in Mice. Based on these favorable pharmacokinetic properties, we evaluated the ability to degrade the PARP1 protein of SK-575 in the SW620 xenograft tumor tissue in mice. Once the tumors had reached 200-300 mm^3, the mice were randomly assigned into the vehicle control group and PROTAC group. The mice were administered a single dose of SK-575 at 25 mg/kg intraperitoneal injection and were sacrificed at 1, 3, 6, and 24 h time-points after treatment. The mice treated with vehicle control were sacrificed at the 3 h time-point. Our western blotting data (Figure 10B) showed that a single dose of SK-575 at 25 mg/kg is very effective in reducing the level of PARP1 protein in xenograft tumor tissue. The degradation of PARP1 protein started at 1 h after treatment and reached the maximum effect at 6 h, indicating a rapid degradation of PARP1 in vivo when compared to the vehicle. Our pharmacodynamics (PD) data thus demonstrates that a single dose of SK-575 at 25 mg/kg is highly effective in inducing near-complete elimination of PARP1 protein in tumor tissue in mice with the effect persisting for 24 h.

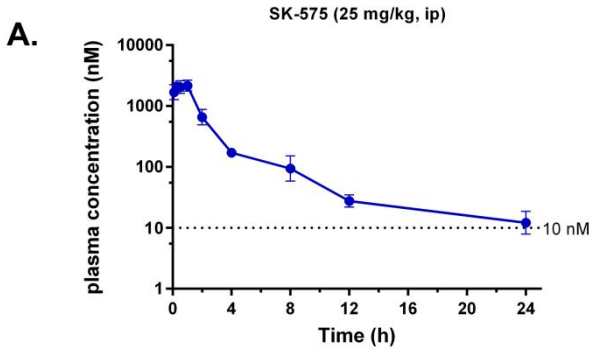

Parameters	Mean
t_{max} (h)	0.25
C_{max} (ng/ml)	1843
AUC_{all} (ng*h/ml)	5316
AUC_{inf} (ng*h/ml)	5363
$t_{1/2}$ (h)	3.08

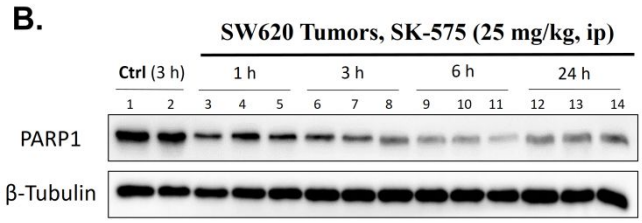

Figure 10. In vivo evaluation of PARP1 degrader SK-575. (A) PK study of SK-575 in mice (n = 3 per group). (B) PD study of SK-575 in SW620 tumor tissue in mice. The treatment groups mice bearing xenograft SW620 tumors were treated with a single dose of SK-575 (25 mg/kg, ip). Tumor tissues were harvested at the indicated time-points for western blotting assay.

Antitumor Effect of SK-575 Administration in Xenograft Tumor Models. Upon the basis of its impressive PK and PD data, we evaluated the efficacy of SK-575 in three xenograft models in mice when used as a single agent or in combination with cytotoxic agents at different doses and schedules.

In the beginning, to assess the in vivo antitumor effects of SK-575 used as a single agent, we treated nude mice bearing established subcutaneous Capan-1 tumor xenograft with SK-575 and obtained the

results shown in Figure 11A. Capan-1 is a human pancreatic cancer cell line with BRCA2 deficient.[58] Olaparib effectively retarded tumor growth over the control, but SK-575 can achieve much similar antitumor activity than olaparib at a lower dosage and fewer times of administration. At the lower dose of 25 mg/kg once daily, the administration of SK-575 for five times a week for 3 weeks intraperitoneally has a similar effect on tumor growth with olaparib (100 mg/kg, oral, daily dosing). SK-575 at these doses (25 and 50 mg/kg) were well tolerated, with no mice lethality or significant weight loss observed during the treatment time (Figure S7 in Supporting Information).

We observed a clear additive effect of combining PARP1 degrader SK-575 with MMS in SW620 cell lines in vitro (Figure 8D). Thus, to assess the antitumor of SK-575 in combination with TMZ in vivo, we used a nude mice colorectal SW620 xenograft model to compare the antitumor activity of TMZ (at 50 mg/kg for 5 days, po, once daily) either alone or in combination with SK-575 (at 5 and 10 mg/kg for 5 days, ip, once daily) or olaparib (at 10 mg/kg for 5 days, po, once daily) as the reference standard (Figure 11B). This dose and schedule of olaparib had previously demonstrated potentiation of TMZ antitumor activity.[18] Our data showed that TMZ alone can suppress tumor growth and the efficacy improved when combined with SK-575 in dose-dependent manners. At a high dose of 10 mg/kg combination with TMZ for 5 consecutive days, SK-575 significantly inhibited tumor regrowth compared with TMZ alone ($P < 0.01$), similarly to the results of olaparib ($P < 0.01$). We examined combinatorial toxicity through body weight loss and the results were shown in Figure S7 in supporting information. Our data indicated that TMZ alone group was well-tolerated with a maximum mean body weight loss of 9% at the 6-day time-point and recovered quickly after treatment. However, body weight loss was greater in the two combination groups of the 10 mg/kg of SK-575 and olaparib, with a maximum mean body weight loss of

15% at the 9-day time-point in these two groups and full recovery within a week. There was no animal lethality during the whole experiment. Overall, our combination therapy of PARP1 degrader was well-tolerated under these doses and schedules. It is worth noting that this is the first preclinical example of PROTAC compounds combined with other drugs for tumor treatment in vivo, which would provide favorable evidence for the clinical application of PROTAC compounds.

We next examined the additive effect of SK-575 when combined with cisplatin in vivo. The nude mice bearing Capan-1 tumor xenografts were treated with SK-575 (at 25 and 50 mg/kg for 5 days, ip, once daily) or olaparib (at 10 mg/kg for 5 days, po, once daily) in combination with a 6 mg/kg intraperitoneal injection of cisplatin at the 2-day time-point (Figure 11C). The nude mice treated with cisplatin alone had antitumor activity， and the efficacy improved when combined with SK-575 in dose-dependent manners. Significant potentiation was observed as early as day 16 ($P = 0.027$) for the combination groups of SK-575 at 50 mg/kg and continued to differentiate from the cisplatin alone group out to day 32 ($P < 0.01$). However, we did note that the combination regimens involving cisplatin resulted in a maximum average body weight loss of 9% and 12% at the 10-day time-point (Figure S7 in Supporting Information), which were observed for groups that contained SK-575 doses of 25 mg/kg and 50 mg/kg, respectively. In the same experiment, the nude mice treated with olaparib and cisplatin also showed combinatorial toxicity, with maximum body weight loss of 11%. Mice recovered their body weight after a week of maximum body weight losing, and no mice lethality was observed.

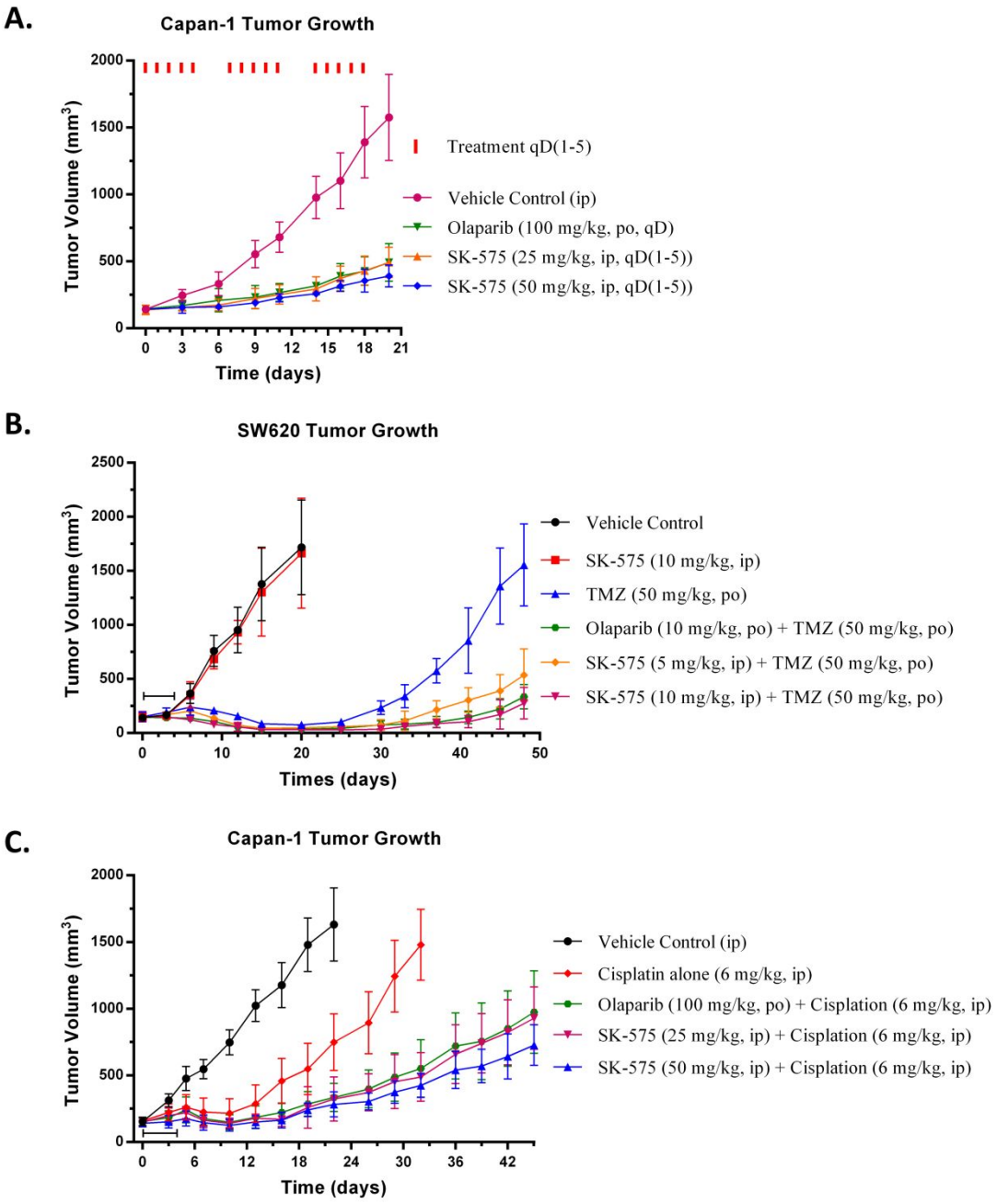

Figure 11. (A) Antitumor efficacy of SK-575 in BRCA2-mutated Capan-1 xenografts (n = 6). (B) Antitumor efficacy of SK-575 in combination with temozolomide (TMZ) in SW620 xenografts (n = 6). Nude mice were dosed once daily for 5 consecutive days (days 0-4 are indicated by a short line). (C) Antitumor efficacy of SK-575 in combination with cisplatin in BRCA2-mutated Capan-1 xenografts (n = 6). Nude mice were dosed SK-575 once daily for 5 consecutive days (days 0-4 are indicated by a short line), and cisplatin was dosed intraperitoneally at 6 mg/kg on the 2-day time-

point. The efficacy of the treatment is expressed as mean ± SEM.

CONCLUSIONS

In conclusion, by linking known PARP1 inhibitor olaparib to E3 ligase ligand (for example, thalidomide and lenalidomide), we have designed and synthesized a series of PARP1 degraders. Through extensive optimization of the length and composition of the linker, we identified compound **18** (SK-575) as a promising PARP1 degrader that exhibits rapid, highly potent and specific degradation of PARP1 protein in various cancer cells with DC_{50} value at concentrations as low as picomolar with a 24 h treatment time. Furthermore, SK-575 can cause persistent depletion of PARP1 protein in MDA-MB-436 cells at 100 nM for 5 days treatment, and the degraded PARP1 protein induced by the pretreatment of SK-575 is rarely recovered after washout it for 24 h. SK-575 displays good potency against PARP1. Our data show that SK-575 can not only effectively inhibit the growth of a variety of tumor cells as a single agent, as exemplified by the MDA-MB-436 and Capan-1 cells, but also potentiate the cell killing by alkylating agent MMS. Significantly, our PK and PD data indicate that a single dose of SK-575 achieves a sufficient exposure in plasma for over 24 h, and effectively induces PARP1 degradation in the SW620 xenograft tumor tissue with the effect persisting for >24 h. Furthermore, SK-575 significantly inhibited the tumor growth in vivo as a single-agent in HR-deficient xenograft models, and synergistic sensitization in combination with cytotoxic agents (TMZ or cisplatin) at well-tolerated dose schedules. Collectively, SK-575 is the most potent and efficacious PARP1 degrader reported to date and warrants further evaluation as a potential new therapy for the treatment of diseases caused by PARP1 hyperactivation.

CHEMISTRY

Compounds **6-11** were synthesized according to the route shown in Scheme 1. Compound **31** was obtained by condensation of 3-hydroxyphthalic anhydride (**29**) and 3-aminopiperidine-2,6-dione hydrochloride (**30**). Compound **31** was alkylated with *tert*-butyl bromate to obtain **32**, which was hydrolyzed in trifluoroacetic acid (TFA) to result in intermediate **33**. Condensation of **34** obtained from commercial source with *N*-Boc-piperazine in the presence of 1-[bis(dimethylamino)methylene]-1*H*-1,2,3-triazolo[4,5-b]-pyridinium 3-oxide hexafluorophosphate (HATU) and triethylamine in dimethylformamide (DMF) afforded the compound **35**. Compounds **36a,b** were prepared with **35** and *N*-Boc-butylamine or *N*-Boc-hexamine using a similar procedure described above. After Bco-deprotection of **36a,b** with HCl in DCM, Compounds **6** and **7** were obtained by condensation of **36a,b** with **33** using a similar method as was used for **35**. Compounds **8-11** were prepared from **36a,b** by the same procedure as was used for the synthesis of **6**.

Scheme 1. Synthesis of Compounds 6-11[a]

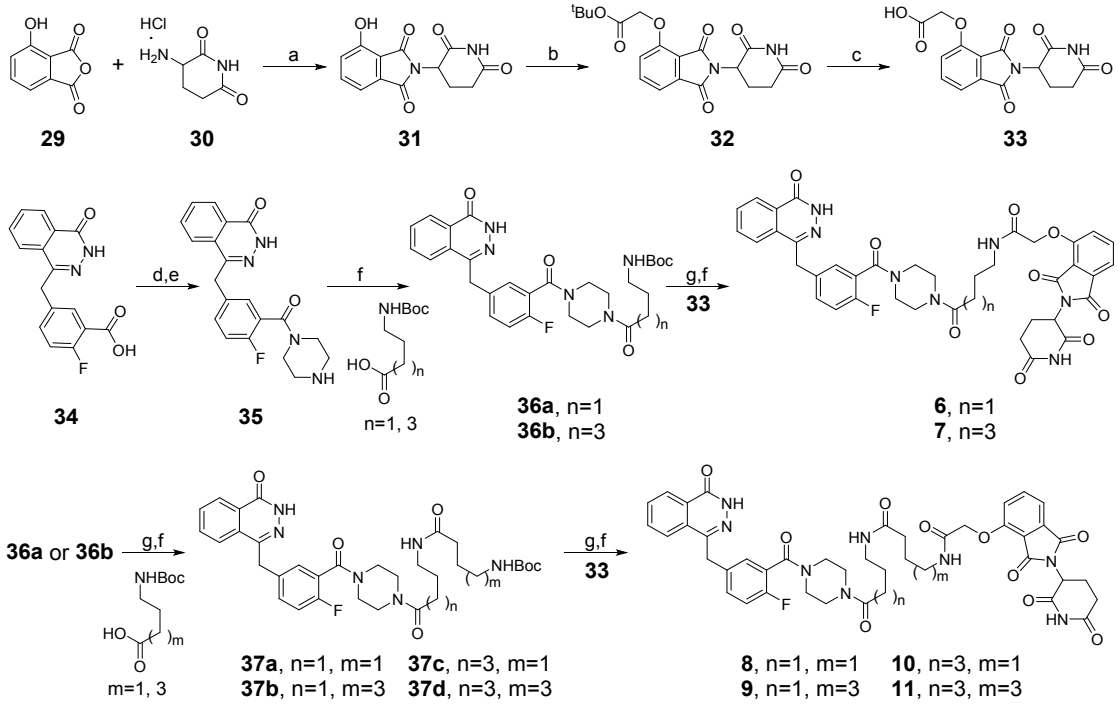

[a]Reaction conditions: (a) TEA, toluene, reflux; (b) *tert*-butyl bromoacetate, KI, $KHCO_3$, DMF, 60 °C; (c) TFA/DCM, rt; (d) *N*-Boc-piperazine, HATU, TEA, DMF, rt; (e) HCl, EtOH, rt; (f) HATU, DIPEA, DMF, rt; (g) HCl, DCM/MeOH, rt.

The synthesis of compounds **12** and **13** is shown in Scheme 2. Condensation of 3-fluorophthalic anhydride (**38a**) with **30** afforded the intermediate **39a**. Compound **40** was synthesized from **39a** by substitution reaction. The *tert*-butyl in **40** was removed in TFA/DCM to obtain compound **41**. Compounds **12** and **13** were prepared from **37a,b** by the same procedure as was used for the synthesis of **6**.

Scheme 2. Synthesis of Compounds 12-13[a]

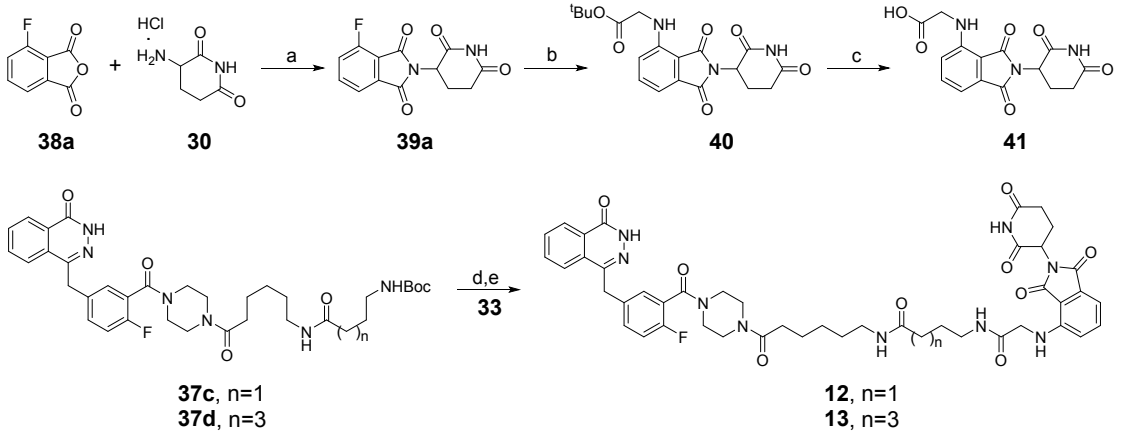

[a]Reaction conditions: (a) NaOAc, AcOH, reflux; (b) *tert*-butyl glycinate, DIPEA, NMP, 90 °C; (c) TFA, DCM, rt; (d) HCl, DCM/MeOH, rt; (e) HATU, DIPEA, DMF, rt.

The synthesis of PARP1 degraders **14-25** is shown in Scheme 3. Compounds **42a-f** were prepared by a substitution reaction of **39a** with different lengths of mono-Boc protected alkyl diamines. Intermediates **43a-g** were synthesized by an amide condensation reaction with **35** and different lengths of alkyl dicarboxylic acid. Condensation of **42a-f** with **43a-g** using previously described methods generated PARP1 degraders **14-25**.

Scheme 3. Synthesis of Compounds 14-25[a]

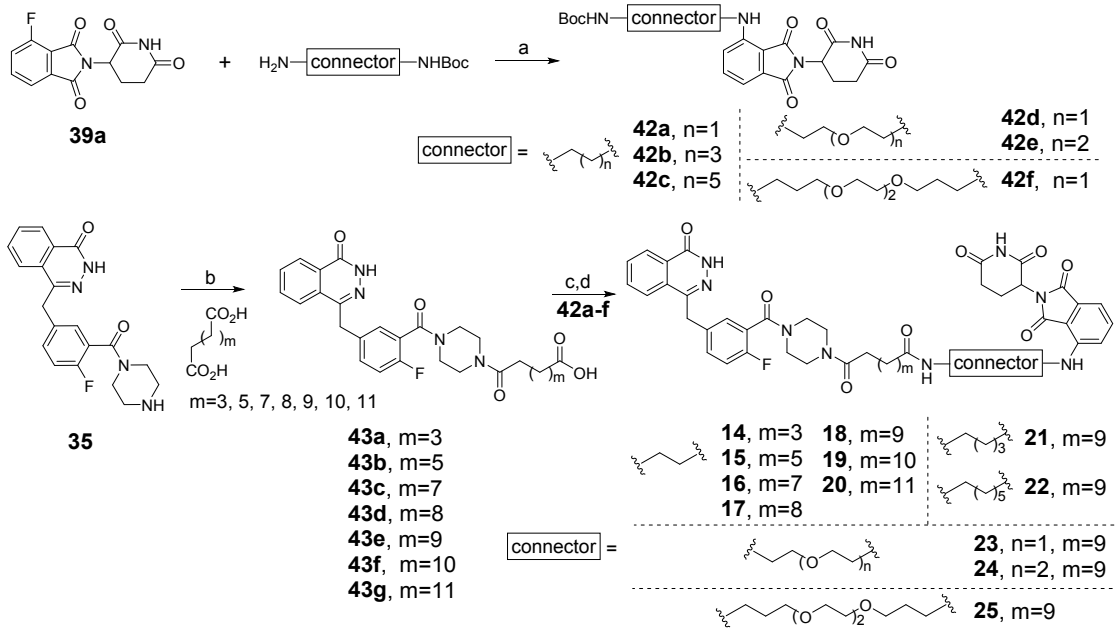

[a]Reaction conditions: (a) DIPEA, NMP, 90 °C; (b) HBTU, DIPEA, DMF, rt; (c) HCl, DCM, MeOH, rt; (d) HATU, DIPEA, DMF, rt.

As shown in Scheme 4, intermediate **44** was obtained from **38b** through two steps by a process similar to that used for the synthesis of **40** from **38a**. Compound **26** was prepared from **43e** using the method used in the preparation of **14-25**.

Scheme 4. Synthesis of Compound 26[a]

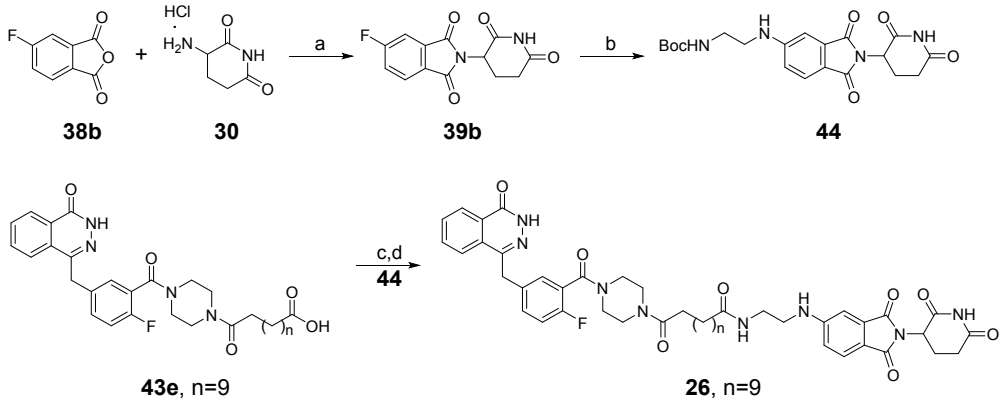

[a]Reaction conditions: (a) NaOAc, AcOH, reflux; (b) *N*-Boc-ethylenediamine, DIPEA, NMP, 90 °C; (c) HCl, DCM, MeOH, rt; (d) HATU, DIPEA, DMF, rt.

The synthesis of compound **27** is shown in Scheme 5. Alkylation of the lenalidomide with *N*-Boc-2-aminoacetaldehyde (**45**) afforded the intermediate **46**. Condensation of **43e** with **46** using the previously described procedure resulting in compound **27**.

Scheme 5. Synthesis of Compound 27[a]

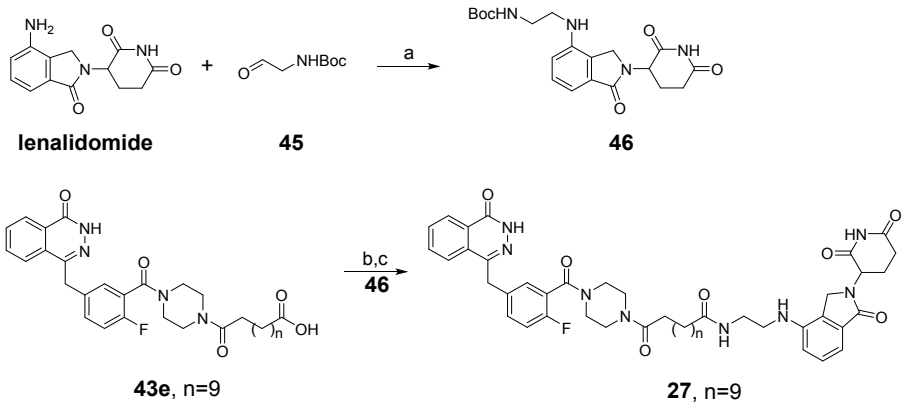

[a]Reaction conditions: (a) $NaBH_3CN$, MeOH, 50 °C; (b) HCl, DCM, MeOH, rt; (c) HATU, DIPEA, DMF, rt.

The synthesis of compound **28** is shown in Scheme 6. Compound **39a** was methylated with MeI to obtain **47**. Compound **48** was obtained by a substitution reaction of **47** with *N*-Boc-ethylenediamine. Compounds **28** was prepared to start from **43e** in the same method as was used for **14-25**.

Scheme 6. Synthesis of Compound 28[a]

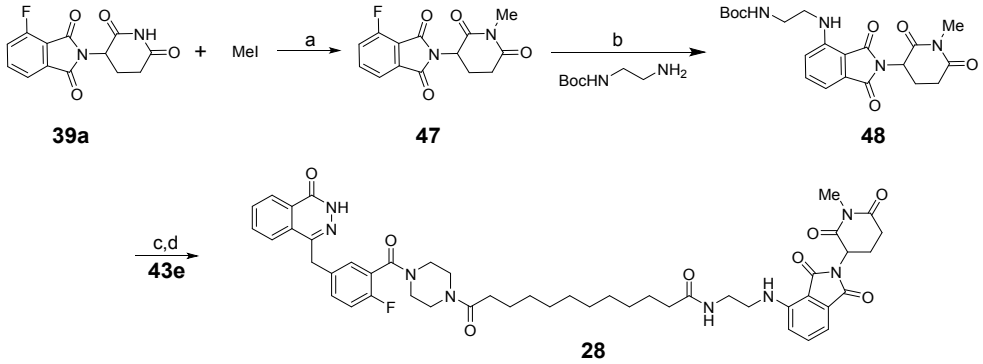

[a]Reaction conditions: (a) MeI, K_2CO_3, DMF, 50 °C; (b) DIPEA, NMP, 90 °C; (c) HCl, DCM, MeOH, rt; (d) HATU,

DIPEA, DMF, rt.

Finally, compounds **29-32** were synthesized according to the route shown in Scheme 7. Following the published procedure for the synthesis of intermediate compounds **49-52**, and the synthetic route were shown in Scheme S1 in supporting information. Condensation of **43e** with **49-52** using previously described methods generated PARP1 degraders **29-32**.

Scheme 7. Synthesis of Compounds 29-32[a]

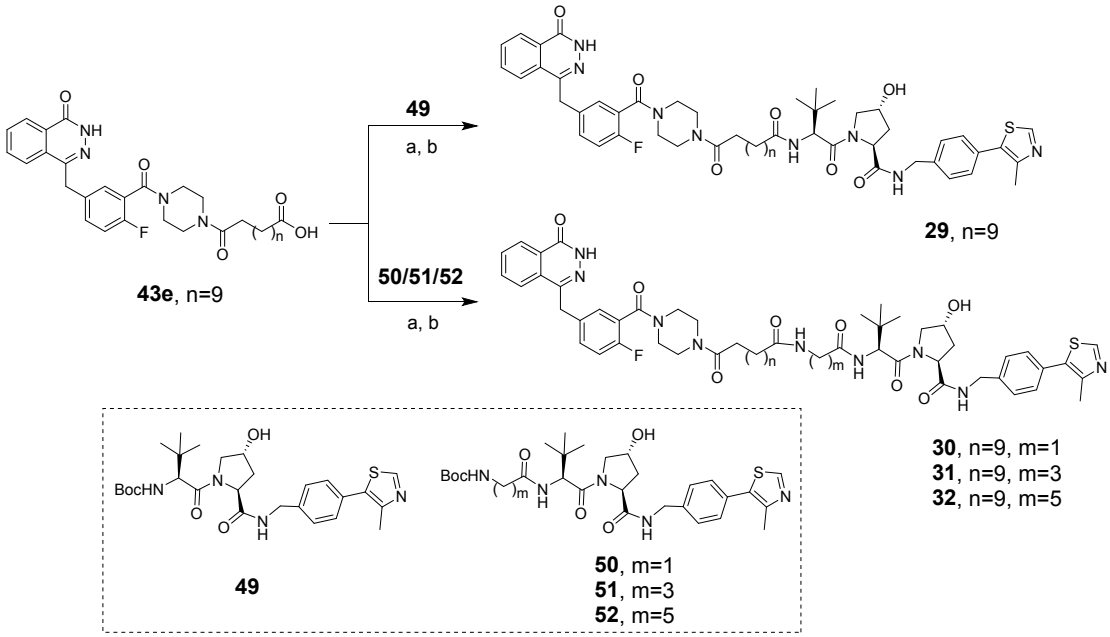

[a]Reaction conditions: (a) HCl, DCM, MeOH, rt; (b) HATU, DIPEA, DMF, rt.

EXPERIMENTAL SECTION

Chemistry: General Information. Unless otherwise noted, all reactions were carried out under atmosphere, and common reagents or materials were obtained from commercial sources and used without further purification. Compound **3** (iRucaparib-AP6) was purchased from the commercial source MedChemExpress. Olaparib, temozolomide (TMZ), and cisplatin were purchased from the commercial

source Adamas-beta®. Flash column chromatography was performed using silica gel from Qindao Haiyang, and its specification was 300-400 mesh. NMR spectra were recorded on a Bruker AMX 400 spectrometer and were calibrated using TMS or residual deuterated solvent as an internal reference ($CDCl_3$: 7.26 ppm for ^1H NMR and 77.16 ppm for ^{13}C NMR; DMSO-*d*6: 2.50 ppm for ^1H NMR and 39.50 ppm for ^{13}C NMR; CD_3OD: 3.31 ppm for ^1H NMR and 49.00 ppm for ^{13}C NMR). In the reported spectral data, all NMR spectra were reported in ppm, and the format (δ) chemical shift (multiplicity, J values in Hz, integration) was described as the following abbreviations: s = singlet, d = doublet, t = triplet, q = quartet, m = multiplet, and br = broadening of peaks, which was often observed due to the slow rotation of the amide bonds. HRMS spectra were recorded on a Waters Q-TOF Premier. The final compounds were all purified by C18 reverse-phase preparative high-performance liquid chromatography (HPLC) column with solvent A [0.1% trifluoroacetic acid (TFA) in water] and solvent B (0.1% TFA in MeCN) as eluents. The purity of all the final compounds was confirmed to be > 95% by HPLC.

2-((2-(2,6-Dioxopiperidin-3-yl)-1,3-dioxoisoindolin-4-yl)oxy)-*N*-(4-(4-(2-fluoro-5-((4-oxo-3,4-dihydrophthalazin-1-yl)methyl)benzoyl)piperazin-1-yl)-4-oxobutyl)acetamide (6). Following the published procedure for the synthesis of compound **33**.[53] In a round bottom flask, 3-aminopiperidine-2,6-dione hydrochloride **29** (1.64 g, 10.0 mmol, 1.0 equiv), 3-hydroxyphthalic anhydride **30** (1.64 g, 10.0 mmol, 1.0 equiv) and triethylamine (1.56 mL, 12.0 mmol, 1.2 equiv) were dissolved in toluene (60 mL). The resulting reaction mixture was heated to reflux in an oil bath for 12 hours. After cooling to the ambient temperature, evaporation of most of the solvent afforded a crude product, which was purified by column chromatography with DCM/EtOAc system to obtain **31** as a white solid (2.41 g, 88% yield). ^1H NMR (400 MHz, DMSO-d_6) δ (ppm) 11.16 (s, 1H), 11.08 (s,1H), 7.65 (t, *J* = 7.6 Hz, 1H), 7.32 (d, *J* = 7.2 Hz,

1H), 7.25 (d, *J* = 8.4 Hz, 1H), 5.07 (dd, *J* = 12.8 Hz, *J* = 5.2 Hz, 1H), 2.93−2.84 (m, 1H), 2.61−2.46 (m, 3H), 2.05−2.01 (m, 1H). ^{13}C NMR (101 MHz, DMSO-d_6) δ (ppm) 172.75, 169.96, 166.98, 165.78, 155.43, 136.35, 133.12, 123.52, 114.34, 114.26, 48.62, 30.93, 22.01.

In a round bottom flask, Compound **31** (1.9 g, 7.0 mmol, 1.0 equiv) was dissolved in DMF (20 mL). KI (116 mg, 0.7 mmol, 0.1 equiv) and $KHCO_3$ (1.05 g, 10.05 mmol, 1.5 equiv) were added to the stirred solution. Then *tert*-butyl bromoacetate (1.24 ml, 8.4 mmol, 1.2 equiv) was added dropwise and the mixture was stirred at 60 °C overnight. EtOAc (200 mL) was added into the reaction mixture, washed with saturated brine, and the combined organic layer was dried over anhydrous Na_2SO_4. After filtrating and decompressing the solvent, the residue was purified by DCM/EtOAc to obtain **32** as a white solid (2.16 g, 85% yield). ^{1}H NMR (400 MHz, $CDCl_3$) δ (ppm) 8.19 (s, 1H), 7.66 (dd, *J* = 8.4, *J* = 7.4 Hz, 1H), 7.50 (d, *J* = 7.3 Hz, 1H), 7.10 (d, *J* = 8.4 Hz, 1H), 5.01−4.92 (m, 1H), 4.78 (s, 2H), 2.93−2.67 (m, 3H), 2.16−2.07 (m, 1H), 1.47 (s, 9H); ^{13}C NMR (101 MHz, $CDCl_3$) δ (ppm) 171.12, 168.09, 167.00, 166.96, 165.57, 155.65, 136.40, 134.04, 119.94, 117.71, 117.03, 83.24, 66.69, 49.31, 31.51, 28.16, 22.70.

In a round bottom flask, **32** (1.7 g, 4.4 mmol) was dissolved in 20 mL TFA/DCM (1:1) and stirred at room temperature for 2 h. After concentration of the solvent, the residue **33** as a white solid was used to the following steps without further purification. ^{1}H NMR (400 MHz, DMSO-d_6) δ (ppm) 13.22 (s, 1H), 11.11 (s, 1H), 7.80 (dd, *J* = 8.6, 7.3 Hz, 1H), 7.48 (d, *J* = 7.2 Hz, 1H), 7.40 (d, *J* = 8.5 Hz, 1H), 5.11 (dd, *J* = 12.9, *J* = 5.4 Hz, 1H), 4.99 (s, 2H), 2.90 (m, 1H), 2.69−2.53 (m, 2H), 2.05 (m, 1H)； ^{13}C NMR (101 MHz, DMSO-*d*6) δ (ppm) 173.24, 170.37, 169.96, 167.20, 165.63, 155.60, 137.22, 133.72, 120.35, 116.79, 116.22, 65.48, 49.26, 31.42, 22.44. HRMS (DART-TOF) calculated for $C_{15}H_{12}N_2NaO_7^+$ [M + Na]$^+$ m/z 355.0542, found 355.0541.

In a round bottom flask, compound **34** (4.45 g, 15 mmol, 1.0 equiv) and *N*-Boc-piperazine (3.35 g, 18 mmol, 1.2 equiv) were dissolved in DMF (100 mL), and the mixture was cooled to 0 °C. Triethylamine (4.2 mL, 30 mmol, 2.0 equiv) and HATU (6.80 g, 18 mmol, 1.2 equiv) were added sequentially to a stirred solution. The resulting mixture was stirred at room temperature for 5 h. Water (500 mL) was added to the reaction solution and stirred at 0 °C for 1 h. A large amount of white solid was obtained by suction filtration, and the filter cake was washed with a small amount of ice water and cold EtOAc to obtain the intermediate crude product (6.43 g, 92% yield).

In a round bottom flask, the intermediate obtained from the previous step (6.43 g, 13.8 mmol) was dissolved in ethanol (50 mL) was added, and then HCl (6 N, 6.9 mL) was added dropwise to a quickly stirred solution. The resulting mixture was stirred at room temperature for 3 h after dropping and then concentrated in vacuo. The pH of the solution was adjusted to >10 with aqueous ammonium hydroxide (4 N). The resulting mixture was extracted with DCM (3 × 100 mL), and then the combined organic layers were washed with brine and dried over anhydrous Na_2SO_4. After filtration and evaporation, the crude residue was purified by flash column chromatography with hexane/EtOAc to obtain **35** as a white solid (4.45 g, 88% yield). ^{1}H NMR (400 MHz, DMSO-d_6) δ (ppm) 12.58 (s, 1H), 8.26 (d, J = 7.7 Hz, 1H), 7.96 (d, J = 7.9 Hz, 1H), 7.88 (t, J = 7.2 Hz, 1H), 7.82 (t, J = 7.4 Hz, 1H), 7.44−7.37 (m, 1H), 7.31 (dd, J = 6.4, J = 1.7 Hz, 1H), 7.20 (t, J = 9.0 Hz, 1H), 5.75 (s, 1H), 4.32 (s, 2H), 3.53 (s, 2H), 3.06 (s, 2H), 2.70 (t, J = 4.8 Hz, 2H), 2.56 (t, J = 4.7 Hz, 2H). HRMS (DART-TOF) calculated for $C_{20}H_{20}FN_4O_2^+$ $[M + H]^+$ m/z 367.1570, found 367.1565.

In a round bottom flask, compound **35** (732 mg, 2.0 mmol, 1.0 equiv) and *N*-Boc-butylamine (406 mg, 2.0 mmol, 1.0 equiv) were dissolved in DMF (10 mL), and the mixture was cooled to 0 °C. DIPEA (0.66

mL, 4.0 mmol, 2.0 equiv) and HATU (836 mg, 2.2 mmol, 1.1 equiv) were added sequentially. The resulting mixture was stirred at room temperature for 3 h and then added brine (100 mL), extracted with EtOAc (3 × 100 mL). The combined organic layers were washed with brine and dried over anhydrous Na_2SO_4. After filtration and evaporation, the crude residue was purified by flash column chromatography with DCM/MeOH (10:1) to obtain **36a** as a white solid (904 mg, 82% yield). ^{1}H NMR (400 MHz, $CDCl_3$) δ (ppm) 11.66 (br, 1H), 8.49−8.37 (m, 1H), 7.71 (dd, *J* = 10.5, *J* = 4.0 Hz, 3H), 7.40−7.22 (m, 2H), 7.00 (dd, *J* = 12.3, *J* = 5.9 Hz, 1H), 4.90 (s, 1H), 4.27 (s, 2H), 3.87−3.21 (m, 8H), 3.14 (m, 2H), 2.39 (t, *J* = 7.1 Hz, 1H), 2.32 (t, *J* = 6.9 Hz, 1H), 1.88−1.74 (m, 2H), 1.39 (m, 9H). HRMS (DART-TOF) calculated for $C_{29}H_{34}FN_5NaO_5^+$ $[M + Na]^+$ m/z 574.2442, found 574.2437.

In a round bottom flask, compound **36a** (121.2 mg, 0.22 mmol, 1.1 equiv) was dissolved in DCM (10 mL) and MeOH (2 mL) and then added HCl (1 mL, 4 M in 1,4-dixoane). After stirring for 2 h, the solvent was evaporated and the residue was used in the next step without further purification. The intermediate obtained from the previous step was dissolved in DMF (10 mL). After cooling to 0 °C, compound **33** (66.4 mg, 0.2 mmol, 1.0 equiv), DIPEA (99 μL, 0.6 mmol, 3.0 equiv) and HATU (76 mg, 0.2 mmol, 1.0 equiv) were added sequentially to a stirred solution. The resulting mixture was stirred at room temperature for 1 h and then added brine (50 mL), extracted with EtOAc (3 × 50 mL). The combined organic layers were washed with brine and dried over anhydrous Na_2SO_4. After filtration and evaporation, the crude residue was purified by flash column chromatography with DCM/MeOH (10:1) to obtain **6** as a white powder (108.6 mg, 71% yield). ^{1}H NMR (400 MHz, $CDCl_3$) δ (ppm) 11.26 (br, 1H), 9.66 (br, 1H), 8.41 (dd, *J* = 6.2, *J* = 1.8 Hz, 1H), 7.78−7.65 (m, 4H), 7.65−7.55 (m, 1H), 7.54−7.46 (m, 1H), 7.37−7.23 (m, 2H), 7.19 (d, *J* = 8.4 Hz, 1H), 7.01 (t, *J* = 8.5 Hz, 1H), 4.98 (m, 1H), 4.64 (s, 2H), 4.26 (s, 2H), 3.85−3.15

(m, 10H), 2.92−2.70 (m, 3H), 2.49−2.31 (m, 2H), 2.13 (s, 1H), 1.98−1.84 (m, 2H). HRMS (DART-TOF) calculated for $C_{39}H_{36}FN_7NaO_9^+$ $[M + Na]^+$ m/z 788.2456, found 788.2458. Purity, 97.2%.

2-((2-(2,6-Dioxopiperidin-3-yl)-1,3-dioxoisoindolin-4-yl)oxy)-*N*-(6-(4-(2-fluoro-5-((4-oxo-3,4-dihydrophthalazin-1-yl)methyl)benzoyl)piperazin-1-yl)-6-oxohexyl)acetamide (**7**). Compound **7** (55.7 mg, 70% yield) was obtained as white powder using the procedure for the synthesis of compound **6** with **36b**. ^{1}H NMR (400 MHz, $CDCl_3$) δ (ppm) 11.13 (br, 1H), 9.85 (br, 1H), 8.48−8.40 (m, 1H), 7.81−7.65 (m, 4H), 7.62−7.48 (m, 2H), 7.35−7.26 (m, 2H), 7.20 (d, *J* = 8.4 Hz, 1H), 7.02 (t, *J* = 8.7 Hz, 1H), 5.08−4.87 (m, 1H), 4.64 (q, *J* = 14.2 Hz, 2H), 4.27 (s, 2H), 3.85−3.15 (m, 10H), 2.93−2.67 (m, 3H), 2.43−2.25 (m, 2H), 2.19−2.09 (m, 1H), 1.72−1.52 (m, 4H), 1.45−1.31 (m, 2H). HRMS (DART-TOF) calculated for $C_{41}H_{40}FN_7NaO_9^+$ $[M + Na]^+$ m/z 816.2769, found 816.2766. Purity, 96.3%.

4-(2-((2-(2,6-Dioxopiperidin-3-yl)-1,3-dioxoisoindolin-4-yl)oxy)acetamido)-*N*-(4-(4-(2-fluoro-5-((4-oxo-3,4-dihydrophthalazin-1-yl)methyl)benzoyl)piperazin-1-yl)-4-oxobutyl)butanamide (**8**). Compound **8** (62.9 mg, 74% yield) was obtained as white powder using the procedure for the synthesis of compound **6** with **37a**. ^{1}H NMR (400 MHz, DMSO-d_6) δ (ppm) 12.58 (s, 1H), 11.11 (s, 1H), 8.26 (dd, *J* = 7.8, *J* = 1.1 Hz, 1H), 7.98 (m, 2H), 7.93−7.85 (m, 1H), 7.86−7.74 (m, 3H), 7.49 (d, *J* = 7.1 Hz, 1H), 7.46-7.33 (m, 3H), 7.23 (t, *J* = 9.0 Hz, 1H), 5.12 (dd, *J* = 12.9, *J* = 5.4 Hz, 1H), 4.76 (d, *J* = 8.6 Hz, 2H), 4.33 (s, 2H), 3.69−2.98 (m, 12H), 2.95−2.82 (m, 1H), 2.66−2.47 (m, 2H), 2.34 (t, *J* = 6.7 Hz, 1H), 2.28 (t, *J* = 7.1 Hz, 1H), 2.14−1.95 (m, 3H), 1.72−1.54 (m, 4H). HRMS (DART-TOF) calculated for $C_{43}H_{43}FN_8NaO_{10}^+$ $[M + Na]^+$ m/z 873.2984, found 873.2984. Purity, 98.1%.

6-(2-((2-(2,6-Dioxopiperidin-3-yl)-1,3-dioxoisoindolin-4-yl)oxy)acetamido)-*N*-(4-(4-(2-fluoro-5-((4-oxo-3,4-dihydrophthalazin-1-yl)methyl)benzoyl)piperazin-1-yl)-4-oxobutyl)hexanamide (**9**).

Compound **9** (71.9 mg, 82% yield) was obtained as white powder using the procedure for the synthesis of compound **6** with **37b**. ^{1}H NMR (400 MHz, $CDCl_3$) δ (ppm) 10.92 (br, 1H), 10.30 (br, 1H), 8.48−8.39 (m, 1H), 7.82−7.66 (m, 4H), 7.61−7.49 (m, 2H), 7.36−7.24 (m, 3H), 7.20 (d, *J* = 8.4 Hz, 1H), 7.03 (t, *J* = 8.8 Hz, 1H), 6.44−6.33 (m, 1H), 4.99 (dd, *J* = 11.9, *J* = 5.6 Hz, 1H), 4.72−4.56 (m, 2H), 4.27 (s, 2H), 3.84−3.13 (m, 12H), 2.92−2.69 (m, 3H), 2.43 (t, *J* = 6.2 Hz, 1H), 2.35 (t, *J* = 6.3 Hz, 1H), 2.26−2.05 (m, 3H), 1.67−1.50 (m, 4H), 1.45−1.32 (m, 3H). HRMS (DART-TOF) calculated for $C_{45}H_{47}FN_8NaO_{10}^+$ [M + Na]$^+$ m/z 901.3297, found 901.3294. Purity, 96.2%.

4-(2-((2-(2,6-Dioxopiperidin-3-yl)-1,3-dioxoisoindolin-4-yl)oxy)acetamido)-*N*-(6-(4-(2-fluoro-5-((4-oxo-3,4-dihydrophthalazin-1-yl)methyl)benzoyl)piperazin-1-yl)-6-oxohexyl)butanamide (**10**). Compound **10** (68.5 mg, 78% yield) was obtained as white powder using the procedure for the synthesis of compound **6** with **37c**. ^{1}H NMR (400 MHz, $CDCl_3$) δ (ppm) 11.23 (br, 1H), 9.75 (s, 1H), 8.42 (dd, *J* = 6.6, *J* = 2.5 Hz, 1H), 7.80−7.62 (m, 5H), 7.51 (d, *J* = 7.3 Hz, 1H), 7.35−7.24 (m, 2H), 7.21 (d, *J* = 8.4 Hz, 1H), 7.02 (t, *J* = 8.7 Hz, 1H), 6.61−6.42 (m, 1H), 5.03−4.89 (m, 1H), 4.65 (s, 2H), 4.27 (s, 2H), 3.82−3.11 (m, 12H), 2.91−2.71 (m, 3H), 2.34 (t, *J* = 7.0 Hz, 1H), 2.26 (t, *J* = 7.1 Hz, 1H), 2.21 (t, *J* = 7.2 Hz, 2H), 2.17−2.14 (m, 1H), 1.93−1.78 (m, 2H), 1.67−1.54 (m, 2H), 1.53−1.41 (m, 2H), 1.39−1.26 (m, 3H). HRMS (DART-TOF) calculated for $C_{45}H_{47}FN_8NaO_{10}^+$ [M + Na]$^+$ m/z 901.3297, found 901.3296. Purity, 95.5%.

6-(2-((2-(2,6-Dioxopiperidin-3-yl)-1,3-dioxoisoindolin-4-yl)oxy)acetamido)-*N*-(6-(4-(2-fluoro-5-((4-oxo-3,4-dihydrophthalazin-1-yl)methyl)benzoyl)piperazin-1-yl)-6-oxohexyl)hexanamide (**11**). Compound **11** (68.8 mg, 76% yield) was obtained as white powder using the procedure for the synthesis of compound **6** with **37d**. ^{1}H NMR (400 MHz, $CDCl_3$) δ (ppm) 11.15 (br, 1H), 10.08 (s, 1H), 8.50−8.38 (m, 1H), 7.81−7.66 (m, 4H), 7.61−7.47 (m, 2H), 7.37−7.26 (m, 3H), 7.20 (d, *J* = 8.4 Hz, 1H), 7.03 (t, *J* =

8.8 Hz, 1H), 6.05 (s, 1H), 5.00 (dd, *J* = 11.7, *J* = 5.9 Hz, 1H), 4.64 (q, *J* = 14.2 Hz, 2H), 4.28 (s, 2H), 3.86−3.11 (m, 13H), 2.95−2.66 (m, 3H), 2.35 (t, *J* = 6.7 Hz, 1H), 2.35 (t, *J* = 7.1 Hz, 1H), 2.24−2.09 (m, 3H), 1.70−1.53 (m, 6H), 1.54−1.42 (m, 2H), 1.43−1.26 (m, 4H). HRMS (DART-TOF) calculated for $C_{47}H_{51}FN_8NaO_{10}^+$ $[M + Na]^+$ m/z 929.3610, found 929.3614. Purity, 98.1%.

4-(2-((2-(2,6-Dioxopiperidin-3-yl)-1,3-dioxoisoindolin-4-yl)amino)acetamido)-*N*-(6-(4-(2-fluoro-5-((4-oxo-3,4-dihydrophthalazin-1-yl)methyl)benzoyl)piperazin-1-yl)-6-oxohexyl)butanamide (**12**). In a round-bottom flask, 3-fluorophthalic anhydride **38a** (3.32 g, 20 mmol, 1.0 equiv), 3-aminopiperidine-2,6-dione hydrochloride **30** (3.29 g, 20 mmol, 1.0 equiv), and sodium acetate (1.97 g, 24 mmol, 1.2 equiv) were disolved in AcOH (100 mL). The resulting mixture was heated to reflux at 120 °C overnight. After cooling to room temperature, the solvent was remolved in vacuo and the residue was poured into water (200 mL), extracted with EtOAc (5 × 100 mL). The combined organic layers were washed with brine and dried over anhydrous Na_2SO_4. After filtration and evaporation, the crude residue was pulped with DCM and then filter to obtain white powder **39a** (4.52 g, 82% yield). ^{1}H NMR (400 MHz, DMSO-d_6) δ (ppm) 11.15 (s, 1H) , 7.98−7.93 (m, 1H) ,7.80−7.72 (m, 2H) , 5.17 (dd, *J* = 13.2 Hz, *J* = 5.2 Hz, 1H) , 2.95−2.86 (m, 1H) , 2.64−2.47 (m, 2H) , 2.10−2.06 (m, 1H).

In a round-bottom flask, compond **39a** (552 mg, 2 mmol, 1.0 equiv), *tert*-butyl glycinate (324 mg, 2.4 mmol, 1.2 equiv), and DIPEA (660 μL, 4 mmol, 2.0 equiv) were disolved in NMP (5 mL). The resulting mixture was heated to reflux at 90 °C overnight. After colling to room temperature, the resulting mixture was poured into water (50 mL) and extracted with EtOAc (3 × 100 mL). The combined organic layers were washed with brine and dried over anhydrous Na_2SO_4. After filtration and evaporation, the crude residue was purified by flash column chromatography with petroleum ether/EtOAc to obtain **40** as a

yellow powder (503 mg, 65% yield). ^{1}H NMR (400 MHz, $CDCl_3$) δ (ppm) 7.57 (dd, *J* = 8.5, *J* = 7.1 Hz, 1H), 7.12 (d, *J* = 7.1 Hz, 1H), 6.94 (d, *J* = 8.5 Hz, 1H), 5.51 (s, 2H), 5.09 (m, 1H), 2.94−2.66 (m, 3H), 2.14 (m, 1H), 1.51 (s, 9H). HRMS (DART-TOF) calculated for $C_{19}H_{21}N_3NaO_6^+$ $[M + Na]^+$ m/z 410.1323, found 410.1326.

In a round bottom flask, **40** (503 mg，1.3 mmol) was dissolved in 20 ml TFA/DCM (1:1) and stirred at room temperature for 2 h. After concentration of the solvent, the residue **41** as a yellow solid was used to the following steps without further purification. ^{1}H NMR (400 MHz, DMSO-d_6) δ (ppm) 12.75 (s, 1H), 11.01 (s, 1H), 7.56 (t, *J* = 8.2 Hz, 1H), 7.18 (d, *J* = 6.80 Hz ,1H), 6.89 (d, *J* = 8.4 Hz, 1H), 6.86 (t, J = 5.6 Hz, 1H), 5.04 (dd, *J* = 13.2 Hz, *J* = 5.8 Hz, 1H), 4.12 (d, *J* = 5.2 Hz, 2H), 2.84−2.75 (m, 1H), 2.73−2.59 (m, 2H), 2.09−2.07 (m, 1H)； ^{13}C NMR (100 MHz, DMSO-d_6) δ (ppm) 172.3, 170.2, 169.8, 169.3, 167.1, 145.5, 137.6, 132.1, 119.2, 110.8, 110.1, 61.0, 49.9, 31.7, 21.5. HRMS (DART-TOF) calculated for $C_{15}H_{13}N_3NaO_6^+$ $[M + Na]^+$ m/z 354.0702, found 354.0768.

Compound **12** (64.0 mg, 73% yield) was obtained as yellow powder using the procedure for the synthesis of compound **6** with **37c**. ^{1}H NMR (400 MHz, $CDCl_3$) δ (ppm) 10.90 (s, 1H), 9.31 (s, 1H), 8.48−8.36 (m, 1H), 7.84−7.66 (m, 3H), 7.49 (t, *J* = 7.5 Hz, 1H), 7.38−7.28 (m, 2H), 7.14 (d, *J* = 6.8 Hz, 1H), 7.05 (t, *J* = 8.7 Hz, 1H), 6.85−6.69 (m, 2H), 6.36−6.24 (m, 1H), 5.02−4.86 (m, 1H), 4.28 (s, 2H), 3.94 (d, *J* = 5.0 Hz, 2H), 3.80−3.11 (m, 12H), 2.95−2.69 (m, 3H), 2.31 (dt, *J* = 12.6, *J* = 6.6 Hz, 2H), 2.19−2.04 (m, 3H), 1.74−1.86 (m, 2H), 1.66−1.56 (m, 2H), 1.43−1.53 (m, 2H), 1.38−1.29 (m, 2H). HRMS (DART-TOF) calculated for $C_{45}H_{48}FN_9NaO_9^+$ $[M + Na]^+$ m/z 900.3451, found 900.3461. Purity, 98.7%.

6-(2-((2-(2,6-Dioxopiperidin-3-yl)-1,3-dioxoisoindolin-4-yl)amino)acetamido)-*N*-(6-(4-(2-fluoro-5-((4-oxo-3,4-dihydrophthalazin-1-yl)methyl)benzoyl)piperazin-1-yl)-6-oxohexyl)hexanamide (**13**).

Compound **13** (73.3 mg, 81% yield) was obtained as yellow powder using the procedure for the synthesis of compound **6** with **37d**. ^{1}H NMR (400 MHz, $CDCl_3$) δ (ppm) 10.96 (s, 1H), 9.39 (s, 1H), 8.49−8.39 (m, 1H), 7.83−7.67 (m, 3H), 7.50 (t, *J* = 7.8 Hz, 1H), 7.38−7.27 (m, 2H), 7.15 (d, *J* = 7.1 Hz, 1H), 7.04 (t, *J* = 8.6 Hz, 1H), 6.97−6.86 (m, 1H), 6.80 (d, *J* = 8.5 Hz, 1H), 6.74 (t, *J* = 5.9 Hz, 1H), 6.04−5.91 (m, 1H), 5.05−4.88 (m, 1H), 4.28 (s, 2H), 3.94 (d, *J* = 5.9 Hz, 2H), 3.82−3.14 (m, 12H), 2.93−2.67 (m, 3H), 2.36 (t, *J* = 6.7 Hz, 1H), 2.28 (t, *J* = 7.1 Hz, 1H), 2.18−2.01 (m, 3H), 1.68−1.40 (m, 8H), 1.37−1.17 (m, 4H). HRMS (DART-TOF) calculated for $C_{47}H_{52}FN_9NaO_9^+$ $[M + Na]^+$ m/z 928.3764, found 928.3767. Purity, 95.9%.

***N*-(2-((2-(2,6-Dioxopiperidin-3-yl)-1,3-dioxoisoindolin-4-yl)amino)ethyl)-6-(4-(2-fluoro-5-((4-oxo-3,4-dihydrophthalazin-1-yl)methyl)benzoyl)piperazin-1-yl)-6-oxohexanamide** (**14**). Compound **14** (39.6 mg, 50% yield) was obtained as yellow powder using the procedure for the synthesis of compound **18** with **42a** and **43a**. ^{1}H NMR (400 MHz, $CDCl_3$) δ (ppm) 11.08 (br, 1H), 9.49 (br, 1H), 8.42 (d, *J* = 6.1 Hz, 1H), 7.86−7.62 (m, 3H), 7.44 (t, *J* = 7.7 Hz, 1H), 7.37−7.26 (m, 2H), 7.13 (s, 1H), 7.07−6.98 (m, 2H), 6.93 (d, *J* = 8.5 Hz, 1H), 6.47 (br, 1H), 4.92 (d, *J* = 5.8 Hz, 1H), 4.27 (s, 2H), 3.85−3.12 (m, 12H), 2.91−2.64 (m, 3H), 2.38 (s, 1H), 2.23 (s, 1H), 2.09 (m, 1H), 1.71−1.49 (m, 4H). HRMS (DART-TOF) calculated for $C_{41}H_{41}FN_8NaO_8^+$ $[M + Na]^+$ m/z 815.2924, found 815.2933. Purity, 96.2%.

***N*-(2-((2-(2,6-Dioxopiperidin-3-yl)-1,3-dioxoisoindolin-4-yl)amino)ethyl)-8-(4-(2-fluoro-5-((4-oxo-3,4-dihydrophthalazin-1-yl)methyl)benzoyl)piperazin-1-yl)-8-oxooctanamide** (**15**). Compound **15** (46.9 mg, 57% yield) was obtained as yellow powder using the procedure for the synthesis of compound **18** with **42a** and **43b**. ^{1}H NMR (400 MHz, $CDCl_3$) δ (ppm) 11.07 (br, 1H), 9.42 (s, 1H), 8.51−8.33 (m, 1H), 7.84−7.62 (m, 3H), 7.44 (t, *J* = 7.4 Hz, 1H), 7.37−7.26 (m, 2H), 7.04 (dd, *J* = 12.5, *J* = 7.8 Hz, 2H), 6.94

(d, J = 8.6 Hz, 1H), 6.51 (br, 1H), 6.40 (s, 1H), 5.01−4.84 (m, 1H), 4.27 (s, 2H), 3.85−3.16 (m, 12H), 2.91−2.67 (m, 3H), 2.33 (t, J = 7.1 Hz, 1H), 2.25 (t, J = 6.8 Hz, 1H), 2.18−2.04 (m, 3H), 1.67−1.46 (m, 4H), 1.35−1.19 (m, 6H). HRMS (DART-TOF) calculated for $C_{43}H_{45}FN_8NaO_8^+$ $[M + Na]^+$ m/z 843.3237, found 843.3234. Purity, 97.3%.

***N*-(2-((2-(2,6-Dioxopiperidin-3-yl)-1,3-dioxoisoindolin-4-yl)amino)ethyl)-10-(4-(2-fluoro-5-((4-oxo-3,4-dihydrophthalazin-1-yl)methyl)benzoyl)piperazin-1-yl)-10-oxodecanamide** (**16**). Compound **16** (46.6 mg, 55% yield) was obtained as yellow powder using the procedure for the synthesis of compound **18** with **42a** and **43c**. ^{1}H NMR (400 MHz, $CDCl_3$) δ (ppm) 11.03 (br, 1H), 9.27 (br, 1H), 8.44 (d, J = 6.4 Hz, 1H), 7.83−7.62 (m, 3H), 7.46 (t, J = 7.7 Hz, 1H), 7.38−7.27 (m, 2H), 7.04 (m, 2H), 6.96 (d, J = 8.5 Hz, 1H), 6.40 (s, 2H), 5.00−4.84 (m, 1H), 4.27 (s, 2H), 3.88−3.09 (m, 12H), 2.90−2.67 (m, 3H), 2.29 (m, 2H), 2.18−2.04 (m, 3H), 1.67−1.46 (m, 4H), 1.36−1.15 (m, 8H). HRMS (DART-TOF) calculated for $C_{45}H_{49}FN_8NaO_8^+$ $[M + Na]^+$ m/z 871.3550, found 871.3554. Purity, 98.5%.

***N*-(2-((2-(2,6-Dioxopiperidin-3-yl)-1,3-dioxoisoindolin-4-yl)amino)ethyl)-11-(4-(2-fluoro-5-((4-oxo-3,4-dihydrophthalazin-1-yl)methyl)benzoyl)piperazin-1-yl)-11-oxoundecanamide** (**17**). Compound **17** (46.6 mg, 55% yield) was obtained as yellow powder using the procedure for the synthesis of compound **18** with **42a** and **43d**. ^{1}H NMR (400 MHz, $CDCl_3$) δ (ppm) 11.18 (br, 1H), 9.32 (br, 1H), 8.49−8.29 (m, 1H), 7.84−7.61 (m, 3H), 7.44 (t, J = 7.8 Hz, 1H), 7.38−7.26 (m, 2H), 7.03 (dd, J = 12.5, J = 7.8 Hz, 2H), 6.95 (t, J = 7.3 Hz, 1H), 6.50 (br, 1H), 6.39 (s, 1H), 4.93 (dd, J = 12.1, J = 5.4 Hz, 1H), 4.26 (s, 2H), 3.89−3.10 (m, 12H), 2.91−2.64 (m, 3H), 2.32 (t, J = 7.1 Hz, 1H), 2.25 (t, J = 6.9 Hz, 1H), 2.19−2.07 (m, 3H), 1.67−1.44 (m, 4H), 1.31−1.15 (m, 10H). HRMS (DART-TOF) calculated for $C_{46}H_{51}FN_8NaO_8^+$ $[M + Na]^+$ m/z 885.3706, found 885.3706. Purity, 96.7%.

***N*-(2-((2-(2,6-Dioxopiperidin-3-yl)-1,3-dioxoisoindolin-4-yl)amino)ethyl)-12-(4-(2-fluoro-5-((4-oxo-3,4-dihydrophthalazin-1-yl)methyl)benzoyl)piperazin-1-yl)-12-oxododecanamide** (**18**). In a round bottom flask, compond **39a** (2.76 g, 10 mmol, 1.0 equiv), *N*-Boc-ethylenediamine (1.76 g, 10.1 mmol, 1.1 equiv) and DIPEA (3.3 mL, 20 mmol, 2.0 equiv) were disolved in NMP (50 mL). The resulting mixture was heated to reflux at 90 °C overnight. After cooling to room temperature, the resulting mixture was poured into water (200 mL) and extracted with EtOAc (3 × 200 mL). The combined organic layers were washed with brine and dried over anhydrous Na_2SO_4. After filtration and evaporation, the crude residue was purified by flash column chromatography with petroleum ether/EtOAc to obtain the intermediate **42a** as a yellow powder (2.74 g, 66% yield). ^{1}H NMR (400 MHz, $CDCl_3$) δ (ppm) 8.04 (s, 1H), 7.50 (dd, J = 8.5, J = 7.1 Hz, 1H), 7.12 (d, J = 7.1 Hz, 1H), 6.98 (d, J = 8.6 Hz, 1H), 6.39 (t, J = 6.0 Hz, 1H), 4.92 (dd, J = 12.1, J = 5.3 Hz, 1H), 4.82 (s, 1H), 3.45 (q, J = 5.9 Hz, 2H), 3.36 (q, J = 5.7 Hz, 2H), 2.92−2.68 (m, 3H), 2.13 (m, 1H), 1.45 (s, 9H). HRMS (DART-TOF) calculated for $C_{20}H_{24}N_4NaO_6^+$ $[M + Na]^+$ m/z 439.1588, found 439.1592.

In a round bottom flask, HBTU (418 mg, 1.1 mmol, 1.1 equiv), dodecanedioic acid (690 mg, 3.0 mmol, 3.0 equiv) and DIPEA (990 μL, 6 mmol, 6.0 equiv) were disolved in DMF (10 mL) and then the mixture was stirred at room temperature for 5 min. Compound **35** (366 mg, 1.0 mmol, 1.0 equiv) was added into the mixture and the resulting mixture stirred at room temperature for 16 h. The resulting mixture was poured into water (50 mL) and extracted with EtOAc (3 × 100 mL). The combined organic layers were washed with brine and dried over anhydrous Na_2SO_4. After filtration and evaporation, the crude residue was purified by flash column chromatography with DCM/MeOH to obtain the intermediate **43e** as a white solid (502.9 mg, 87% yield). ^{1}H NMR (400 MHz, $CDCl_3$) δ (ppm) 11.83 (br, 1H), 8.44 (d, J = 6.5 Hz,

1H), 7.74 (m, 3H), 7.31 (m, 2H), 7.02 (t, J = 8.8 Hz, 1H), 4.28 (s, 2H), 3.91−3.14 (m, 8H), 2.33 (m, 4H), 1.69−1.52 (m, 4H), 1.37−1.18 (m, 12H). HRMS (DART-TOF) calculated for $C_{32}H_{39}FN_4NaO_5^+$ $[M + Na]^+$ m/z 601.2802, found 601.2802.

In a round bottom flask, compound **42a** (45.8 mg, 0.11 mmol, 1.1 equiv) was dissolved in DCM (10 mL) and MeOH (2 mL) and then added HCl (1 mL, 4 M in 1,4-dixoane). After stirring for 2 h, the solvent was evaporated and the residue was used in the next step without further purification. The intermediate obtained from the previous step, compound **43e** (57.8 mg, 0.1 mmol, 1.0 equiv) and DIPEA (33 μL, 0.2 mmol, 2.0 equiv) was dissolved in DMF (10 mL). After cooling to 0 °C, HATU (38 mg, 0.1 mmol, 1.0 equiv) were added sequentially to a stirred solution. The resulting mixture was stirred at room temperature for 1 h and then added brine (50 mL), extracted with EtOAc (3 × 50 mL). The combined organic layers were washed with brine and dried over anhydrous Na_2SO_4. After filtration and evaporation, the crude residue was purified by flash column chromatography with DCM/MeOH (10:1) to obtain **18** as a yellow powder (50.8 mg, 58% yield). ^{1}H NMR (400 MHz, $CDCl_3$) δ (ppm) 11.17 (br, 1H), 9.29 (s, 1H), 8.42 (d, J = 6.4 Hz, 1H), 7.85−7.61 (m, 3H), 7.44 (t, J = 7.7 Hz, 1H), 7.37−7.25 (m, 2H), 7.14−6.99 (m, 2H), 6.96 (d, J = 8.5 Hz, 1H), 6.47 (br, 1H), 6.39 (s, 1H), 4.96−4.82 (m, 1H), 4.26 (s, 2H), 3.86−3.10 (m, 12H), 2.90−2.65 (m, 3H), 2.33 (t, J = 6.7 Hz, 1H), 2.26 (t, J = 6.4 Hz, 1H), 2.17−2.06 (m, 3H), 1.67−1.45 (m, 4H), 1.33−1.09 (m, 12H). HRMS (DART-TOF) calculated for $C_{47}H_{53}FN_8NaO_8^+$ $[M + Na]^+$ m/z 899.3863, found 899.3861. Purity, 96.3%.

***N*-(2-((2-(2,6-Dioxopiperidin-3-yl)-1,3-dioxoisoindolin-4-yl)amino)ethyl)-13-(4-(2-fluoro-5-((4-oxo-3,4-dihydrophthalazin-1-yl)methyl)benzoyl)piperazin-1-yl)-13-oxotridecanamide** (**19**). Compound **19** (56.9 mg, 64% yield) was obtained as yellow powder using the procedure for the synthesis of compound **18**

with **42a** and **43f**. ^{1}H NMR (400 MHz, $CDCl_3$) δ (ppm) 11.05 (br, 1H), 9.15 (br, 1H), 8.48−8.34 (m, 1H), 7.82−7.63 (m, 3H), 7.51−7.40 (m, 1H), 7.38−7.27 (m, 2H), 7.04 (m, 2H), 6.97 (d, *J* = 8.6 Hz, 1H), 6.38 (m, 2H), 4.93 (m, 1H), 4.27 (s, 2H), 3.88−3.17 (m, 12H), 2.92−2.67 (m, 3H), 2.34 (t, *J* = 7.3 Hz, 1H), 2.26 (t, *J* = 7.3 Hz, 1H), 2.20−2.04 (m, 3H), 1.66−1.46 (m, 4H), 1.33−1.15 (m, 14H). HRMS (DART-TOF) calculated for $C_{48}H_{55}FN_8NaO_8^+$ $[M + Na]^+$ m/z 913.4019, found 913.4028. Purity, 97.2%.

***N*-(2-((2-(2,6-Dioxopiperidin-3-yl)-1,3-dioxoisoindolin-4-yl)amino)ethyl)-14-(4-(2-fluoro-5-((4-oxo-3,4-dihydrophthalazin-1-yl)methyl)benzoyl)piperazin-1-yl)-14-oxotetradecanamide** (**20**). Compound **20** (60.6 mg, 67% yield) was obtained as yellow powder using the procedure for the synthesis of compound **18** with **42a** and **43g**. ^{1}H NMR (400 MHz, $CDCl_3$) δ (ppm) 10.90 (d, *J* = 31.1 Hz, 1H), 9.03 (br, 1H), 8.51−8.36 (m, 1H), 7.84−7.62 (m, 3H), 7.50−7.41 (m, 1H), 7.37−7.27 (m, 2H), 7.11−6.91 (m, 3H), 6.47−6.36 (m, 1H), 6.28 (s, 1H), 4.93 (dd, *J* = 12.0, *J* = 5.5 Hz, 1H), 4.27 (s, 2H), 3.92−3.10 (m, 12H), 2.93−2.65 (m, 3H), 2.34 (t, *J* = 7.4 Hz, 1H), 2.27 (t, *J* = 7.1 Hz, 1H), 2.19−2.06 (m, 3H), 1.68−1.50 (m, 4H), 1.31−1.13 (m, 16H). HRMS (DART-TOF) calculated for $C_{49}H_{57}FN_8NaO_8^+$ $[M + Na]^+$ m/z 927.4176, found 927.4189. Purity, 98.5%.

***N*-(4-((2-(2,6-Dioxopiperidin-3-yl)-1,3-dioxoisoindolin-4-yl)amino)butyl)-12-(4-(2-fluoro-5-((4-oxo-3,4-dihydrophthalazin-1-yl)methyl)benzoyl)piperazin-1-yl)-12-oxododecanamide** (**21**). Compound **21** (56.0 mg, 62% yield) was obtained as yellow powder using the procedure for the synthesis of compound **18** with **42b** and **43e**. ^{1}H NMR (400 MHz, $CDCl_3$) δ (ppm) 11.33 (br, 1H), 9.26 (s, 1H), 8.43 (d, *J* = 5.9 Hz, 1H), 7.78−7.64 (m, 3H), 7.44 (t, *J* = 7.7 Hz, 1H), 7.37−7.27 (m, 2H), 7.03 (d, *J* = 6.8 Hz, 2H), 6.84 (d, *J* = 8.5 Hz, 1H), 6.20 (s, 1H), 5.93 (s, 1H), 4.97−4.84 (m, 1H), 4.26 (s, 2H), 3.87−3.11 (m, 12H), 2.90−2.66 (m, 3H), 2.32 (s, 1H), 2.25 (s, 1H), 2.15−2.04 (m, 3H), 1.74−1.46 (m, 8H), 1.36−1.11 (m, 14H).

HRMS (DART-TOF) calculated for $C_{49}H_{57}FN_8NaO_8^+$ $[M + Na]^+$ m/z 927.4181, found 927.4186. Purity, 98.4%.

***N*-(6-((2-(2,6-Dioxopiperidin-3-yl)-1,3-dioxoisoindolin-4-yl)amino)hexyl)-12-(4-(2-fluoro-5-((4-oxo-3,4-dihydrophthalazin-1-yl)methyl)benzoyl)piperazin-1-yl)-12-oxododecanamide (22)**. Compound **22** (60.6 mg, 65% yield) was obtained as yellow powder using the procedure for the synthesis of compound **18** with **42c** and **43e**. ^{1}H NMR (400 MHz, $CDCl_3$) δ (ppm) 11.02 (br, 1H), 8.96 (br, 1H), 8.53−8.36 (m, 1H), 7.88−7.62 (m, 3H), 7.46 (t, *J* = 7.8 Hz, 1H), 7.39−7.27 (m, 2H), 7.13−6.96 (m, 2H), 6.85 (d, *J* = 8.5 Hz, 1H), 6.21 (t, *J* = 5.4 Hz, 1H), 5.75 −5.54 (m, 1H), 4.92 (dd, *J* = 11.7, *J* = 5.3 Hz, 1H), 4.27 (s, 2H), 3.89−3.12 (m, 12H), 2.91−2.66 (m, 3H), 2.44−2.30 (t, *J* = 7.2 Hz, 1H), 2.23−2.29 (t, *J* = 6.8 Hz, 1H), 2.19−2.04 (m, 3H), 1.71−1.54 (m, 6H), 1.53−1.45 (m, 2H), 1.44−1.18 (m, 16H). HRMS (DART-TOF) calculated for $C_{51}H_{61}FN_8NaO_8^+$ $[M + Na]^+$ m/z 955.4489, found 955.4496. Purity, 97.7%.

***N*-(2-(2-((2-(2,6-Dioxopiperidin-3-yl)-1,3-dioxoisoindolin-4-yl)amino)ethoxy)ethyl)-12-(4-(2-fluoro-5-((4-oxo-3,4-dihydrophthalazin-1-yl)methyl)benzoyl)piperazin-1-yl)-12-oxododecanamide (23)**. Compound **23** (39.5 mg, 49% yield) was obtained as yellow powder using the procedure for the synthesis of compound **18** with **42d** and **43e**. ^{1}H NMR (400 MHz, $CDCl_3$) δ (ppm) 10.77 (br, 1H), 8.97 (br, 1H), 8.52−8.41 (m, 1H), 7.86−7.63 (m, 3H), 7.56−7.44 (m, 1H), 7.37−7.27 (m, 2H), 7.10 (d, *J* = 7.1 Hz, 1H), 7.03 (t, *J* = 8.7 Hz, 1H), 6.91 (d, *J* = 8.5 Hz, 1H), 6.56 (t, *J* = 5.3 Hz, 1H), 6.17 (s, 1H), 4.91 (dd, *J* = 12.0, *J* = 5.3 Hz, 1H), 4.28 (s, 2H), 3.94−3.15 (m, 16H), 2.97−2.65 (m, 3H), 2.34 (t, *J* = 7.3 Hz, 1H), 2.27 (t, *J* = 7.0 Hz, 1H), 2.21−2.05 (m, 3H), 1.65−1.49 (m, 4H), 1.32−1.12 (m, 12H). HRMS (DART-TOF) calculated for $C_{49}H_{57}FN_8NaO_9^+$ $[M + Na]^+$ m/z 943.4125, found 943.4136. Purity, 98.1%.

***N*-(2-(2-(2-((2-(2,6-Dioxopiperidin-3-yl)-1,3-dioxoisoindolin-4-yl)amino)ethoxy)ethoxy)ethyl)-12-(4-**

(2-fluoro-5-((4-oxo-3,4-dihydrophthalazin-1-yl)methyl)benzoyl)piperazin-1-yl)-12-oxododecanamide (**24**). Compound **24** (55.9 mg, 58% yield) was obtained as yellow powder using the procedure for the synthesis of compound **18** with **42e** and **43e**. ^{1}H NMR (400 MHz, $CDCl_3$) δ (ppm) 10.66 (br, 1H), 9.05 (br, 1H), 8.51-8.37 (m, 1H), 7.83−7.66 (m, 3H), 7.55−7.42 (m, 1H), 7.38−7.27 (m, 2H), 7.09 (d, *J* = 7.1 Hz, 1H), 7.04 (t, *J* = 8.6 Hz, 1H), 6.89 (d, *J* = 8.5 Hz, 1H), 6.51 (t, *J* = 5.4 Hz, 1H), 6.08 (s, 1H), 4.97−4.84 (m, 1H), 4.28 (s, 2H), 3.95−3.07 (m, 20H), 2.92−2.64 (m, 3H), 2.34 (t, *J* = 7.4 Hz, 1H), 2.27 (t, *J* = 7.1 Hz, 1H), 2.19−2.06 (m, 3H), 1.69−1.48 (m, 4H), 1.33−1.16 (m, 12H). HRMS (DART-TOF) calculated for $C_{51}H_{61}FN_8NaO_{10}^+$ [M + Na]$^+$ m/z 987.4387, found 987.4396. Purity, 96.6%.

***N*-(3-(2-(2-(3-((2-(2,6-Dioxopiperidin-3-yl)-1,3-dioxoisoindolin-4-yl)amino)propoxy)ethoxy)ethoxy)propyl)-12-(4-(2-fluoro-5-((4-oxo-3,4-dihydrophthalazin-1-yl)methyl)benzoyl)piperazin-1-yl)-12-oxododecanamide** (**25**). Compound **25** (55.9 mg, 54% yield) was obtained as yellow powder using the procedure for the synthesis of compound **18** with **42f** and **43e**. ^{1}H NMR (400 MHz, $CDCl_3$) δ (ppm) 10.82 (br, 1H), 8.95 (br, 1H), 8.53−8.35 (m, 1H), 7.83−7.61 (m, 3H), 7.47 (t, *J* = 7.8 Hz, 1H), 7.38−7.27 (m, 2H), 7.15−6.97 (m, 2H), 6.91 (d, *J* = 8.6 Hz, 1H), 6.44 (t, *J* = 5.5 Hz, 1H), 6.22 (s, 1H), 4.96−4.84 (m, 1H), 4.27 (s, 2H), 3.97−3.08 (m, 24H), 2.91−2.65 (m, 3H), 2.34 (t, *J* = 7.3 Hz, 1H), 2.26 (t, *J* = 6.9 Hz, 1H), 2.19−2.04 (m, 3H), 1.96−1.88 (m, 2H), 1.79−1.70 (m, 2H), 1.66−1.49 (m, 4H), 1.35−1.17 (m, 12H). HRMS (DART-TOF) calculated for $C_{55}H_{69}FN_8NaO_{11}^+$ [M + Na]$^+$ m/z 1059.4962, found 1059.4962. Purity, 95.8%.

***N*-(2-((2-(2,6-Dioxopiperidin-3-yl)-1,3-dioxoisoindolin-5-yl)amino)ethyl)-12-(4-(2-fluoro-5-((4-oxo-3,4-dihydrophthalazin-1-yl)methyl)benzoyl)piperazin-1-yl)-12-oxododecanamide** (**26**). Compound **26** (58.7 mg, 67% yield) was obtained as yellow powder using the procedure for the synthesis of compound

18 with **44** and **43e**. ^{1}H NMR (400 MHz, $CDCl_3$) δ (ppm) 10.95 (br, 1H), 9.14 (br, 1H), 8.50−8.35 (m, 1H), 7.85−7.64 (m, 3H), 7.51 (d, *J* = 8.2 Hz, 1H), 7.37−7.27 (m, 2H), 7.04 (t, *J* = 8.5 Hz, 1H), 6.86 (d, *J* = 1.8 Hz, 1H), 6.68 (dd, *J* = 8.4, *J* = 1.9 Hz, 1H), 6.41 (t, *J* = 5.9 Hz, 1H), 5.74 (t, *J* = 4.6 Hz, 1H), 4.94 (dd, *J* = 11.9, *J* = 5.4 Hz, 1H), 4.28 (s, 2H), 3.93-3.13 (m, 12H), 2.93−2.63 (m, 3H), 2.34 (t, *J* = 7.1 Hz, 1H), 2.27 (t, *J* = 6.8 Hz, 1H), 2.22−2.07 (m, 3H), 1.68−1.47 (m, 4H), 1.32−1.15 (m, 12H). HRMS (DART-TOF) calculated for $C_{47}H_{53}FN_8NaO_8^+$ $[M + Na]^+$ m/z 899.3863, found 899.3866. Purity, 96.6%.

***N*-(2-((2-(2,6-Dioxopiperidin-3-yl)-1-oxoisoindolin-4-yl)amino)ethyl)-12-(4-(2-fluoro-5-((4-oxo-3,4-dihydrophthalazin-1-yl)methyl)benzoyl)piperazin-1-yl)-12-oxododecanamide (27)**. Compound **27** (52.6 mg, 61% yield) was obtained as yellow powder using the procedure for the synthesis of compound **18** with **46** and **43e**. ^{1}H NMR (400 MHz, CD_3OD) δ (ppm) 8.41−8.33 (m, 1H), 7.94 (d, *J* = 7.8 Hz, 1H), 7.90−7.77 (m, 2H), 7.53−7.45 (m, 1H), 7.39 (br, 1H), 7.32 (dd, *J* = 10.4, *J* = 5.0 Hz, 1H), 7.16 (t, *J* = 9.0 Hz, 1H), 7.08 (dd, *J* = 7.2, *J* = 4.3 Hz, 1H), 6.86 (d, *J* = 8.0 Hz, 1H), 5.27-5.08 (d, *J* = 11.6 Hz, 1H), 4.38 (s, 2H), 4.27 (s, 2H), 3.85−3.40 (m, 8H), 3.39−3.25 (m, 4H), 3.00−2.84 (m, 1H), 2.84−2.71 (m, 1H), 2.56−2.30 (m, 3H), 2.19 (t, *J* = 7.3 Hz, 3H), 1.72−1.47 (m, 4H), 1.35−1.12 (m, 12H). HRMS (DART-TOF) calculated for $C_{47}H_{55}FN_8NaO_7^+$ $[M + Na]^+$ m/z 885.4070, found 885.4074. Purity, 98.0%.

12-(4-(2-Fluoro-5-((4-oxo-3,4-dihydrophthalazin-1-yl)methyl)benzoyl)piperazin-1-yl)-*N*-(2-((2-(1-methyl-2,6-dioxopiperidin-3-yl)-1,3-dioxoisoindolin-4-yl)amino)ethyl)-12-oxododecanamide (28). Compound **28** (50.7 mg, 57% yield) was obtained as yellow powder using the procedure for the synthesis of compound **18** with **48** and **43e**. ^{1}H NMR (400 MHz, $CDCl_3$) δ (ppm) 10.73 (br, 1H), 8.53−8.33 (m, 1H), 7.86−7.62 (m, 3H), 7.48 (t, *J* = 7.8 Hz, 1H), 7.38−7.27 (m, 2H), 7.14−6.94 (m, 3H), 6.39 (s, 1H), 6.07 (br, 1H), 4.92 (dd, *J* = 12.1, *J* = 5.5 Hz, 1H), 4.27 (s, 2H), 3.88−3.22 (m, 12H), 3.19 (s, 3H), 3.01−2.89

(m, 1H), 2.82−2.68 (m, 2H), 2.34 (t, *J* = 7.0 Hz, 1H), 2.27 (t, *J* = 6.7 Hz, 1H), 2.16 (t, *J* = 7.6 Hz, 2H), 2.11−2.02 (m, 1H), 1.67−1.51 (m, 4H), 1.35−1.17 (m, 12H). HRMS (DART-TOF) calculated for $C_{48}H_{55}FN_8NaO_8^+$ $[M + Na]^+$ m/z 913.4019, found 913.4026. Purity, 96.5%.

(2*S*,4*R*)-1-((*S*)-2-(12-(4-(2-Fluoro-5-((4-oxo-3,4-dihydrophthalazin-1-yl)methyl)benzoyl)piperazin-1-yl)-12-oxododecanamido)-3,3-dimethylbutanoyl)-4-hydroxy-*N*-(4-(4-methylthiazol-5-yl)benzyl)pyrrolidine-2-carboxamide (29). Compound **29** (61.7 mg, 76% yield) was obtained as white powder from **43e** and **49** using the procedure for the synthesis of compound **22**. ^{1}H NMR (400 MHz, $CDCl_3$) δ (ppm) 11.68 (s, 1H), 8.64 (s, 1H), 8.46−8.35 (m, 1H), 7.78−7.63 (m, 3H), 7.57 (s, 1H), 7.30 (q, *J* = 8.3 Hz, 6H), 6.98 (t, *J* = 8.7 Hz, 1H), 6.68 (s, 1H), 4.71 (t, *J* = 7.9 Hz, 1H), 4.64−4.47 (m, 3H), 4.30 (dd, *J* = 15.1, 5.2 Hz, 1H), 4.26−4.12 (m, 3H), 4.07 (d, *J* = 11.2 Hz, 1H), 3.87−3.08 (m, 9H), 2.67−2.36 (m, 5H), 2.35−2.04 (m, 5H), 1.65−1.45 (m, 4H), 1.31−1.11 (m, 12H), 0.94 (s, 9H). HRMS (DART-TOF) calculated for $C_{54}H_{67}FN_8NaO_7S^+$ $[M+Na]^+$ m/z 1013.4735, found 1013.4732. Purity, 96.4%.

(2*S*,4*R*)-1-((*S*)-2-(2-(12-(4-(2-Fluoro-5-((4-oxo-3,4-dihydrophthalazin-1-yl)methyl)benzoyl)piperazin-1-yl)-12-oxododecanamido)acetamido)-3,3-dimethylbutanoyl)-4-hydroxy-*N*-(4-(4-methylthiazol-5-yl)benzyl)pyrrolidine-2-carboxamide (30). Compound **30** (41.2 mg, 55% yield) was obtained as white powder from **43e** and **50** using the procedure for the synthesis of compound **22**. ^{1}H NMR (400 MHz, $CDCl_3$) δ (ppm) 11.60 (s, 1H), 8.64 (s, 1H), 8.46−8.34 (m, 1H), 8.07 (s, 1H), 7.79−7.60 (m, 4H), 7.38−7.22 (m, 6H), 7.06−6.88 (m, 2H), 4.77 (t, *J* = 8.0 Hz, 1H), 4.71 (d, *J* = 9.1 Hz, 1H), 4.55 (dd, *J* = 15.5, 6.6 Hz, 2H), 4.36−4.21 (m, 3H), 4.16 (s, 1H), 4.04−3.93 (m, 3H), 3.81−3.13 (m, 9H), 2.46 (s, 3H), 2.36−2.20 (m, 5H), 2.21−2.09 (m, 2H), 1.65−1.45 (m, 4H), 1.28−1.13 (m, 12H), 0.98 (s, 9H). HRMS (DART-TOF) calculated for $C_{56}H_{70}FN_9NaO_8S^+$ $[M+Na]^+$ m/z 1070.4950, found 1070.4953. Purity,

98.3%.

(2*S*,4*R*)-1-((*S*)-2-(4-(12-(4-(2-Fluoro-5-((4-oxo-3,4-dihydrophthalazin-1-yl)methyl)benzoyl)piperazin-1-yl)-12-oxododecanamido)butanamido)-3,3-dimethylbutanoyl)-4-hydroxy-*N*-(4-(4-methylthiazol-5-yl)benzyl)pyrrolidine-2-carboxamide (31). Compound **31** (55.6 mg, 57% yield) was obtained as white powder from **43e** and **51** using the procedure for the synthesis of compound **22**. ^{1}H NMR (400 MHz, $CDCl_3$) δ (ppm) 11.59 (br, 1H), 8.58 (s, 1H), 8.40−8.24 (m, 1H), 7.77−7.60 (m, 3H), 7.58 (t, *J* = 5.7 Hz, 1H), 7.24 (q, *J* = 8.4 Hz, 6H), 6.95 (d, *J* = 8.4 Hz, 1H), 6.42 (t, *J* = 5.2 Hz, 1H), 4.67 (t, *J* = 8.0 Hz, 1H), 4.53−4.40 (m, 3H), 4.33 (s, 1H), 4.25 (dd, *J* = 15.2, 5.2 Hz, 1H), 4.18 (s, 2H), 4.02 (d, *J* = 11.1 Hz, 1H), 3.78−3.01 (m, 12H), 2.38 (s, 3H), 2.34−2.23 (m, 2H), 2.23−2.07 (m, 4H), 2.02 (t, *J* = 6.0 Hz, 2H), 1.73−1.61 (m, 2H), 1.59−1.35 (m, 3H), 1.31 (d, *J* = 6.6 Hz, 2H), 1.19−1.07 (m, 10H), 0.90 (s, 9H). HRMS (DART-TOF) calculated for $C_{58}H_{74}FN_9NaO_8S^+$ $[M+Na]^+$ m/z 1098.5263, found 1098.5257. Purity, 97.6%.

(2*S*,4*R*)-1-((*S*)-2-(6-(12-(4-(2-Fluoro-5-((4-oxo-3,4-dihydrophthalazin-1-yl)methyl)benzoyl)piperazin-1-yl)-12-oxododecanamido)hexanamido)-3,3-dimethylbutanoyl)-4-hydroxy-*N*-(4-(4-methylthiazol-5-yl)benzyl)pyrrolidine-2-carboxamide (32). Compound **32** (63.1 mg, 69% yield) was obtained as white powder from **43e** and **52** using the procedure for the synthesis of compound **22**. ^{1}H NMR (400 MHz, $CDCl_3$) δ 11.70 (s, 1H), 8.63 (s, 1H), 8.40 (d, *J* = 6.9 Hz, 1H), 7.81−7.58 (m, 4H), 7.30 (dd, *J* = 17.7, 9.2 Hz, 6H), 6.99 (d, *J* = 8.1 Hz, 1H), 6.86 (s, 1H), 6.10 (s, 1H), 4.71 (t, *J* = 7.9 Hz, 1H), 4.66−4.48 (m, 3H), 4.48−4.36 (m, 1H), 4.31 (dd, *J* = 15.4, 5.3 Hz, 1H), 4.24 (s, 2H), 4.07 (d, *J* = 10.9 Hz, 1H), 3.83−3.17 (m, 10H), 3.12 (d, *J* = 6.1 Hz, 2H), 2.53 (s, 2H), 2.44 (s, 3H), 2.42−2.12 (m, 5H), 2.07 (t, *J* = 7.3 Hz, 2H), 1.65−1.45 (m, 6H), 1.45−1.34 (m, 2H), 1.32−1.12 (m, 14H), 0.94 (s, 9H). HRMS (DART-TOF) calculated

for $C_{60}H_{78}FN_9NaO_8S^+$ $[M+Na]^+$ m/z 1126.5576, found 1126.5576. Purity, 98.8%.

Cell Lines and Culture Methods. MDA-MB-436, Capan-1, HCC1937, SW620, MDA-MB-468, MDA-MB-231, PC-3, 22Rv1, LNCaP, L-O2, HEK-293, NCM460, HUV-EC, MCF-10A, and H9c2 cell lines were obtained from the American Type Culture Collection (ATCC) or Cell bank of Chinese Academy of Sciences (CCAS, China). MDA-MB-436, HCC1937, SW620, 22Rv1 and LNCaP cell lines were cultured in RPMI-1640 (HyClone, SH30809.01B) medium supplemented with 10% (v/v) fetal bovine serum (FBS, Gemini, 900108) and 1% (v/v) penicillin-streptomycin (HyClone, SV30010). MDA-MB-468, MDA-MB-231， L-O2, HEK-293, NCM460, HUV-EC, MCF-10A, and H9c2 cells were cultured in DMEM (HyClone, SH30022.01B) media supplemented with 10% (v/v) fetal bovine serum and 1% (v/v) penicillin-streptomycin. Capan-1 cells were cultured in IMDM (HyClone, SH32559.01B) media supplemented with 20% (v/v) fetal bovine serum and 1% (v/v) penicillin-streptomycin. PC-3 cells were cultured in DME/F12 (1:1) (HyClone, SH30026.01B) media supplemented with 10% (v/v) fetal bovine serum and 1% (v/v) penicillin-streptomycin. All cells were grown in a humidified incubator at 37 °C, 5% CO_2.

Cell Growth Inhibition Assays. Cells were grown at 37 °C, 95% air, 5% CO_2 until about 70% confluent, and sub-cultured at least twice before the experiment. Cells were seeded in 96-well plates at individual density in 80 μL of culture medium for 24 h. The cell seeding numbers for individual cell lines were as follows: MDA-MB-436 (700/well), Capan-1 (700/well), HCC1937 (1000/well), SW620 (1000/well), MDA-MB-468 (1500/well), MDA-MB-231 (1500/well), PC-3 (700/well), 22Rv1 (1000/well) and LNCaP (1200/well). Compounds were prepared as 10 mM stock solution in 100% DMSO and were tested in 10-dose IC_{50} mode with a 3-fold serial dilution with culture medium (20 μL) starting at 10-20

μM. After the addition of the tested compounds, the plates were incubated for approximately 7 days (Capan-1 for 13 days) at 37 °C, 95% air, 5% CO_2 after dosing. The 10 μL Cell Counting Kit-8 (CCK-8, SAB, CP002) reagent was added to the well, incubated for at least 1-3 h, and measured at 450 nm via spectrophotometry (Thermo Multiskan MK3). Data were calculated from two wells as the mean percentage of cell growth relative to DMSO-only wells, and the IC_{50} was calculated by nonlinear regression analysis using GraphPad Prism v6.0 software.

Potentiation of MMS Cytotoxicity by SK-575 Determined by the Use of SW620 Cells Growth Assays. SW620 cells (1000/well) were seeded in 96-well plates in 80 μL of growth medium and were left to attach for 24 h. Cells were preincubated with vehicle control (DMSO) or with a single concentration of SK-575 (3, 10, 100 or 300 nM, 10 μL) for 1 h prior to the addition of MMS (0, 1.5 3, 5, 7, 10, 12, and 15 μg/mL, 10 μL), which were diluted with culture medium. Cells were incubated in the presence of each drug combination for 5 days before cell growth was quantified by the use of a CCK-8 assay by measuring the medium's absorbance at 450 nm via spectrophotometry (Thermo Multiskan MK3). The data were calculated from three wells as the mean percentage of cell growth relative to DMSO-only wells.

Western Blotting Analysis. Cells ($5\times10^5 - 9\times10^5$) were seeded in 6-well plates at individual density for 24 h and then were treated with DMSO or compounds at the indicated concentrations for various times, or isolated tumor samples were immediately frozen and ground with a mortar in liquid nitrogen. Cells were washed with cold PBS and lysed in RIPA buffer containing protease inhibitors (MCE, HY-K0010). The lysate was centrifuged (13000 rpm, 4 °C, 15 min); the protein concentrations were determined by the BCA Assay Kit (Beyotime, p0012s). A total of 20-30 μg proteins were loaded onto 7.5-12.5% SDS-PAGE gel and then transferred onto polyvinylidene fluoride (PVDF, Millipore)

membranes. The membranes were blocked for 1 h and incubated with primary antibodies overnight at 4 °C, then washed three times with TBST for 10 min. After incubating with secondary HRP antibody for 2 h at room temperature, the membranes were washed three times with TBST for 10 min and then exposed on autoradiograph films using enhanced chemiluminescence. Software GelQuant.NET (provided by biochemlabsolutions.com.) was used to quantify the percentage of PARP1 degradation. The primary antibodies used were PARP1 (1/1000 dilution, CST#9532), PARP2 (1/1000 dilution, ABS#140704), γH2AX (1/1000 dilution, CST#9718) and β-tubulin (1/1000 dilution, CST#5536).

In vitro PARP1 Activity Assays. Kinase Activity assays were performed at Reaction Biology Corp. as previously described.[18] In brief, compounds were tested in consecutive 3-fold dilution starting from 10 μM, 10 points, in duplicate. Enzyme assay was conducted in reaction buffer containing 50 mM Tris-HCl (pH 8.0), 50 mM NaCl, 10 mM $MgCl_2$, 1 mM DTT, 1% DMSO, and 20 g/ml activated DNA. PARP1 (20 μM) was added into reaction buffer and gently mix. The various compounds were added into the reaction mixture by using Acoustic Technology (Echo 550, LabCyte Inc. Sunnyvale, CA) and incubated for 20 min at 25 °C. Reactions were initiated by adding ^{32}P-NAD^+ (10 μM) into system, which were incunated for 2 h at 25 °C. After deliver reaction mixture to filter-paper and washout free NAD^+ with 0.75% phosphoric acid, the signal was immediately measured by chemiluminescence on a Synergy microplate reader (Bio-Tek). The data was analyzed using Excel and GraphPad Prism v6.0 software for IC_{50} curve fits.

Pharmacokinetics Determination. The pharmacokinetic properties were determined at XPiscoric lnc., China. We carried out pharmacokinetics determinations using female ICR mice (20−23 g, 6-7 week-old, N = 3 per group, purchased Beijing HFK Bioscience Co. ltd., Beijing, China). SK-575 was formulated in

5% (v/v) DMSO, 15% Solutol HS15 and 80% (v/v) D5W and administered intraperitoneally at a single dose of 25 mg/kg. Plasma samples were collected at 0.5, 1, 2, 4, 6, 8, and 24 h after drug treatment (n = 3). Methanol was added to precipitate protein, and the samples were vortexed for 120 s, centrifuged (12000 rpm, 10 minutes, 4 ^{o}C), absorbed supernatant, and the concentrations of compound determined by LC-MS/MS according to a standard curve.

Mouse Xenograft Experiments. Animal studies were conducted under the approval of the Experimental Animal Management Committee of Sichuan University (IACUC number: 20100318). The model was established by the transplantation of Capan-1(5×10^6) or SW620 (6×10^6) cells in 0.1 ml media that were subcutaneously injected into the right armpit of each of the 5-6 week-old male BALB/c nude mice, obtained from Beijing HFK Bioscience Co. ltd., Beijing, China. When the average tumor volume reached approximately 150 mm^3, the mice were selected on the basis of tumor volume and body weight and randomly assigned to treatment groups and vehicle control groups with six animals in each group. Tumor volumes and body weight were measured 2−3 times per week, and tumor volumes were calculated as the formula [length/2] × [$width^2$].

Tumor Proliferation Inhibition Test. SK-575, olaparib and TMZ were dissolved in the vehicle containing 5% (v/v) DMSO, 20% (v/v) PEG400, 10% (v/v) Cremophor EL and 65% (v/v) normal saline (NS). Cisplatin was dissolved in normal saline (NS). In the single-agent studies for Capan-1 xenograft (6 mice per group), olaparib (100 mg/kg) was administered by oral gavage once daily for 21 consecutive days. SK-575 (25 and 50 mg/kg) and vehicle were administered intraperitoneally, once daily for five times per week for 3 weeks. In the TMZ combination studies for SW620 xenograft (6 mice per group), olaparib (10 mg/kg) by oral gavage, SK-575 (5 and 10 mg/kg) and vehicle by intraperitoneal injection was

administered once daily for 5 days starting on day 1. TMZ (50 mg/kg) or its vehicle was administered orally once daily for 5 consecutive days starting on day 0, 45 minutes after olaparib or SK-575 were administered. In the cisplatin combination studies for Capan-1 xenograft (6 mice per group), olaparib (100 mg/kg) by oral gavage, SK-575 (25 and 50 mg/kg) and vehicle by intraperitoneal injection were administered once daily for 5 days starting on day 0. Cisplatin (6 mg/kg) or its vehicle was administered by intraperitoneal injection on day 2, 45 minutes after olaparib or SK-575 were administered.

ASSOCIATED CONTENT

Supporting Information

Chemical structure of the five previously reported PARP1/2 PAOTAC; Western blotting analysis of PARP1 and PARP2 in cancer cell lines treated with indicated compounds; cell growth inhibition activity of SK-575 and olaparib in cancer cell lines and normal cell lines; body weight changes in mice; ^{1}H NMR spectrum for SK-575; HPLC results for SK-575 (PDF)

Molecular formula strings and some data (CSV)

AUTHOR INFORMATION

Corresponding Authors

*(L.Z.) Phone: +86-28-85164063. E-mail: lifengzhao@scu.edu.cn.

*(Y.C.) Phone: +86-28-85503817. E-mail: ywchen@scu.edu.cn.

ORCID

Yuan-Wei Chen: 0000-0003-4248-3613

Author Contributions

[▽]Chaoguo Cao, Jie Yang and Yong Chen contributed equally to this work.

Notes

The authors declare no competing financial interest.

Acknowledgments

We thank Dr. Wu Du, Dr. Jiang Yu, Dr. Ying-Wei Wang and Dr. Li-Feng Zhao for helpful discussions and suggestions. This work was supported by the National Natural Science Foundation of China (No. 81672951) and Chengdu Industrial Cluster Collaborative Innovation Project (2016-XT00-00024-GX).

ABBREVIATIONS USED

BRCA, breast cancer susceptibility genes; BRE, base excision repair; CRBN, cereblon; D5W, dextrose (5%) in water; DCM, dichloromethane; DIPEA, *N*,*N*-diisopropylethylamine; DMA, *N*,*N*-dimethylacetamide; DMF, dimethylformamide; DMSO, dimethyl sulfoxide; HATU, hexafluorophosphate azabenzotriazole tetramethyl uronium; HR, homologous recombination; MMS, methyl methanesulphonate; NAD^+, nicotinamide adenine dinucleotide; NAE, NEDD8-activating enzyme; NS, normal saline; PAR, poly(ADP-ribose); PARP, Poly(ADP ribose) polymerase; PBS, phosphate-buffered saline; PD, pharmacodynamics; PEG, polyethylene glycol; PK, pharmacokinetics; PPIs, protein-protein interactions; PROTAC, proteolysis targeting chimera; PTEN, phosphate and tension homolog deleted on chromosome ten; SSBs, single-strand breaks; TEA, triethylamine; TMZ, temozolomide

REFERENCES

(1) Kleine, H.; Poreba, E.; Lesniewicz, K.; Hassa, P. O.; Hottiger, M. O.; Litchfield, D. W.; Shilton, B. H.; Lüscher, B. Substrate-assisted catalysis by PARP10 limits its activity to mono-ADP-ribosylation. *Mol. Cell* **2008**, *32*, 57-69.

(2) Rouleau, M.; Patel, A.; Hendzel, M. J.; Kaufmann, S. H.; Poirier, G. G. PARP inhibition: PARP1 and beyond. *Nat. Rev. Cancer* **2010**, *10*, 293-301.

(3) Ame, J. C.; Spenlehauer, C.; de Murcia, G. The PARP superfamily. *Bioessays* **2004**, *26*, 882-893.

(4) Evans, J. E.; Frostholm, A.; Rotter, A. Embryonic and postnatal expression of four gamma-aminobutyric acid transporter mRNAs in the mouse brain and leptomeninges. *J. Comp. Neurol.* **1996**, *376*, 431-446.

(5) Jagtap, P.; Szabo, C. Poly(ADP-ribose) polymerase and the therapeutic effects of its inhibitors. *Nat. Rev. Drug Discov.* **2005**, *4*, 421-440.

(6) Schreiber, V.; Dantzer, F.; Ame, J. C.; de Murcia, G. Poly(ADP-ribose): novel functions for an old molecule. *Nat Rev. Mol. Cell Biol.* **2006**, *7*, 517-528.

(7) Durkacz, B. W.; Omidiji, O.; Gray, D. A.; Shall, S. (ADP-ribose)n participates in DNA excision repair. *Nature* **1980**, *283*, 593-596.

(8) Alexander, B. Poly(ADP-ribose). The most elaborate metabolite of NAD+. *The FEBS J.* **2005**, *272*, 4576-4589.

(9) Gibson, B. A.; Kraus, W. L. New insights into the molecular and cellular functions of poly(ADP-ribose) and PARPs. *Nat. Rev. Mol. Cell Biol.* **2012**, *13*, 411-424.

(10) Wang, Z. Q.; Auer, B.; Stingl, L.; Berghammer, H.; Haidacher, D.; Schweiger, M.; Wagner, E. F.

Mice lacking ADPRT and poly(ADP-ribosyl)ation develop normally but are susceptible to skin disease. *Genes Dev.* **1995**, *9*, 509-520.

(11) de Murcia, J. M.; Niedergang, C.; Trucco, C.; Ricoul, M.; Dutrillaux, B.; Mark, M.; Oliver, F. J.; Masson, M.; Dierich, A.; LeMeur, M.; Walztinger, C.; Chambon, P.; de Murcia, G. Requirement of poly(ADP-ribose) polymerase in recovery from DNA damage in mice and in cells. *Proc. Natl. Acad. Sci. U. S. A.* **1997**, *94*, 7303-7307.

(12) Tentori, L.; Graziani, G. Chemopotentiation by PARP inhibitors in cancer therapy. *Pharmacol Res.* **2005**, *52*, 25-33.

(13) Rodon, J.; Iniesta, M. D.; Papadopoulos, K. Development of PARP inhibitors in oncology. *Exp. Opin Inv. Drugs* **2009**, *18*, 31-43.

(14) Ratnam, K.; Low, J. A. Current development of clinical inhibitors of poly(ADP-ribose) polymerase in oncology. *Clin. Cancer Res.* **2007**, *13*, 1383-1388.

(15) Narod, S. A.; Foulkes, W. D. BRCA1 and BRCA2: 1994 and beyond. *Nat. Rev. Cancer* **2004**, *4*, 665-676.

(16) Farmer, H.; McCabe, N.; Lord, C. J.; Tutt, A. N.; Johnson, D. A.; Richardson, T. B.; Santarosa, M.; Dillon, K. J.; Hickson, I.; Knights, C.; Martin, N. M. B.; Jackson, S. P.; Smith, G. C. M.; Ashworth, A. Targeting the DNA repair defect in BRCA mutant cells as a therapeutic strategy. *Nature* **2005**, *434*, 917-921.

(17) Bryant, H. E.; Schultz, N.; Thomas, H. D.; Parker, K. M.; Flower, D.; Lopez, E.; Kyle, S.; Meuth, M.; Curtin, N. J.; Helleday, T. Specific killing of BRCA2-deficient tumours with inhibitors of poly(ADP-ribose) polymerase. *Nature* **2005**, *434*, 913-917.

(18) Menear, K. A.; Adcock, C.; Boulter, R.; Cockcroft, X. L.; Copsey, L.; Cranston, A.; Dillon, K. J.; Drzewiecki, J.; Garman, S.; Gomez, S.; Javaid, H.; Kerrigan, F.; Knights, C.; Lau, A.; Loh, V. M., Jr.; Matthews, I. T.; Moore, S.; O'Connor, M. J.; Smith, G. C.; Martin, N. M. 4-[3-(4-Cyclopropanecarbonylpiperazine-1-carbonyl)-4-fluorobenzyl]-2*H*-phthalazin- 1-one: a novel bioavailable inhibitor of poly(ADP-ribose) polymerase-1. *J. Med. Chem.* **2008**, *51*, 6581-6591.

(19) Sun, Y.; Ding, H.; Liu, X.; Li, X.; Li, L. INPP4B overexpression enhances the antitumor efficacy of PARP inhibitor AG014699 in MDA-MB-231 triple-negative breast cancer cells. *Tumor Biol.* **2014**, *35*, 4469-4477.

(20) Jones, P.; Wilcoxen, K.; Rowley, M.; Toniatti, C. Niraparib: a poly(ADP-ribose) polymerase (PARP) inhibitor for the treatment of tumors with defective homologous recombination. *J. Med. Chem.* **2015**, *58*, 3302-3314.

(21) Shen, Y.; Rehman, F. L.; Feng, Y.; Boshuizen, J.; Bajrami, I.; Elliott, R.; Wang, B.; Lord, C. J.; Post, L. E.; Ashworth, A. BMN 673, a novel and highly potent PARP1/2 inhibitor for the treatment of human cancers with DNA repair deficiency. *Clin. Cancer Res.* **2013**, *19*, 5003-5015.

(22) Curtin, N. J.; Szabo, C. Therapeutic applications of PARP inhibitors: anticancer therapy and beyond. *Mol. Aspects Med.* **2013**, *34*, 1217-1256.

(23) Robson, M.; Im S. A.; Senkus, E.; Xu, B.; Domchek, S. M.; Masuda N.; Delaloge, S.; Li, W.; Tung, N.; Armstrong, A.; Wu. W.; Goessl, C.; Runswick, S.; Conte, P. Olaparib for metastatic breast cancer in patients with a germline BRCA mutation. *N. Engl. J. Med.* **2017**, *377*, 523-533.

(24) Pommier, Y.; O'Connor, M. J.; de Bono, J. Laying a trap to kill cancer cells: PARP inhibitors and their mechanisms of action. *Sci. Transl. Med.* **2016**, *8*, 362ps17.

(25) Murai, J.; Pommier, Y. PARP trapping beyond homologous recombination and platinum sensitivity in cancers. *Ann. Rev. Cancer Biol.* **2019**, *3*, 131-150.

(26) Lord, C. J.; Ashworth, A. PARP inhibitors: synthetic lethality in the clinic. *Science* **2017**, *355*, 1152-1158.

(27) Endres, M.; Wang, Z. Q.; Namura, S.; Waeber, C.; Moskowitz, M. A. Ischemic brain injury is mediated by the activation of poly(ADP-ribose)polymerase. *J. Cereb. Blood Flow Metab.* **1997**, *17*, 1143-1151.

(28) Eliasson, M. J.; Sampei, K.; Mandir, A. S.; Hurn, P. D.; Traystman, R. J.; Bao, J.; Pieper, A.; Wang, Z. Q.; Dawson, T. M.; Snyder, S. H.; Dawson, V. L. Poly(ADP-ribose) polymerase gene disruption renders mice resistant to cerebral ischemia. *Nat. Med.* **1997**, *3*, 1089-1095.

(29) Pieper, A. A.; Walles, T.; Wei, G.; Clements, E. E.; Verma, A.; Snyder, S. H.; Zweier, J. L. Myocardial postischemic injury is reduced by polyADPripose polymerase-1 gene disruption. *Mol. Med.* **2000**, *6*, 271-282.

(30) Zheng, J.; Devalaraja-Narashimha, K.; Singaravelu, K.; Padanilam, B. J. Poly(ADP-ribose) polymerase-1 gene ablation protects mice from ischemic renal injury. *Am. J. Physiol Renal Physiol* **2005**, *288*, 387-398.

(31) Yang, Z.; Zingarelli, B.; Szabo, C. Effect of genetic disruption of poly(ADP-ribose) synthetase on delayed production of inflammatory mediators and delayed necrosis during myocardial ischemia-reperfusion injury. *Shock* **2000**, *13*, 60-66.

(32) Szabó, C. Role of poly(ADP-ribose)synthetase in inflammation. *Tren. Pharm. Sci.* **1998**, 19, 287-298.

(33) Damien, D. A.; Serge, D.; Icy, D. S.; Guy, P. G. Poly(ADP-ribosyl)ation reactions in the regulation of nuclear functions. *Biochem. J.* **1999**, *342*, 249-268.

(34) Fatokun, A. A.; Dawson, V. L.; Dawson, T. M. Parthanatos: mitochondrial-linked mechanisms and therapeutic opportunities. *Br. J. Pharmacol* **2014**, *171*, 2000-2016.

(35) Berger, N. A.; Besson, V. C.; Boulares, A. H.; Burkle, A.; Chiarugi, A.; Clark, R. S.; Curtin, N. J.; Cuzzocrea, S.; Dawson, T. M.; Dawson, V. L.; Hasko, G.; Liaudet, L.; Moroni, F.; Pacher, P.; Radermacher, P.; Salzman, A. L.; Snyder, S. H.; Soriano, F. G.; Strosznajder, R. P.; Sumegi, B.; Swanson, R. A.; Szabo, C. Opportunities for the repurposing of PARP inhibitors for the therapy of non-oncological diseases. *Br. J. Pharmacol* **2018**, *175*, 192-222.

(36) Sakamoto, K. M.; Kim, K. B.; Kumagai, A.; Mercurio, F.; Crews, C. M.; Deshaies, R. J. Protacs: chimeric molecules that target proteins to the Skp1-Cullin-F box complex for ubiquitination and degradation. *Proc. Natl. Acad. Sci. U. S. A.* **2001**, *98*, 8554-8559.

(37) Toure, M.; Crews, C. M. Small-Molecule PROTACS: new approaches to protein degradation. *Angew. Chem., Int. Ed.* **2016**, *55*, 1966-1973.

(38) Winter, G. E.; Buckley, D. L.; Paulk, J.; Roberts, J. M.; Souza, A.; Dhe-Paganon, S.; Bradner, J. E. Phthalimide conjugation as a strategy for in vivo target protein degradation. *Science* **2015**, *348*, 1376-1381.

(39) Zengerle, M.; Chan, K.-H.; Ciulli, A. Selective small molecule induced degradation of the BET bromodomain protein BRD4. *ACS Chem. Biol.* **2015**, *10*, 1770-1777.

(40) Zhou, B.; Hu, J.; Xu, F.; Chen, Z.; Bai, L.; Fernandez-Salas, E.; Lin, M.; Liu, L.; Yang, C.-Y.; Zhao, Y.; McEachern, D.; Przybranowski, S.; Wen, B.; Sun, D.; Wang, S. Discovery of a small-molecule

degrader of bromodomain and extra-terminal (BET) proteins with picomolar cellular potencies and capable of achieving tumor regression. *J. Med. Chem.* **2018**, *61*, 462-481.

(41) Raina, K.; Lu, J.; Qian, Y.; Altieri, M.; Gordon, D.; Rossi, A. M. K.; Wang, J.; Chen, X.; Dong, H.; Siu, K.; Winkler, J. D.; Crew, A. P.; Crews, C. M.; Coleman, K. G. PROTAC-induced BET protein degradation as a therapy for castration-resistant prostate cancer. *Proc. Natl. Acad. Sci. U. S. A.* **2016**, *113*, 7124-7129.

(42) Qin, C.; Hu, Y.; Zhou, B.; Fernandez-Salas, E.; Yang, C.-Y.; Liu, L.; McEachern, D.; Przybranowski, S.; Wang, M.; Stuckey, J.; Meagher, J.; Bai, L.; Chen, Z.; Lin, M.; Yang, J.; Ziazadeh, D. N.; Xu, F.; Hu, J.; Xiang, W.; Huang, L.; Li, S.; Wen, B.; Sun, D.; Wang, S. Discovery of QCA570 as an exceptionally potent and efficacious proteolysis targeting chimera (PROTAC) degrader of the bromodomain and extra-terminal (BET) proteins capable of inducing complete and durable tumor regression. *J. Med. Chem.* **2018**, *61*, 6685-6704.

(43) Han, X.; Wang, C.; Qin, C.; Xiang, W.; Fernandez-Salas, E.; Yang, C.-Y.; Wang, M.; Zhao, L.; Xu, T.; Chinnaswamy, K.; Delproposto, J.; Stuckey, J.; Wang, S. Discovery of ARD-69 as a highly potent proteolysis targeting chimera (PROTAC) degrader of androgen receptor (AR) for the treatment of prostate cancer. *J. Med. Chem.* **2019**, *62*, 941-964.

(44) Hu, J.; Hu, B.; Wang, M.; Xu, F.; Miao, B.; Yang, C.-Y.; Wang, M.; Liu, Z.; Hayes, D. F.; Chinnaswamy, K.; Delproposto, J.; Stuckey, J.; Wang, S. Discovery of ERD-308 as a highly potent proteolysis targeting chimera (PROTAC) degrader of estrogen receptor (ER). *J. Med. Chem.* **2019**, *62*, 1420-1442.

(45) Zhang, C.; Han, X. R.; Yang, X.; Jiang, B.; Liu, J.; Xiong, Y.; Jin, J. Proteolysis targeting chimeras

(PROTACs) of anaplastic lymphoma kinase (ALK). *Eur. J. Med. Chem.* **2018**, *151*, 304-314.

(46) Olson, C. M.; Jiang, B.; Erb, M. A.; Liang, Y.; Doctor, Z. M.; Zhang, Z.; Zhang, T.; Kwiatkowski, N.; Boukhali, M.; Green, J. L.; Haas, W.; Nomanbhoy, T.; Fischer, E. S.; Young, R. A.; Bradner, J. E.; Winter, G. E.; Gray, N. S. Pharmacological perturbation of CDK9 using selective CDK9 inhibition or degradation. *Nat. Chem. Biol.* **2018**, *14*, 163-170.

(47) Robb, C. M.; Contreras, J. I.; Kour, S.; Taylor, M. A.; Abid, M.; Sonawane, Y. A.; Zahid, M.; Murry, D. J.; Natarajan, A.; Rana, S. Chemically induced degradation of CDK9 by a proteolysis targeting chimera (PROTAC). *Chem. Commun.* **2017**, *53*, 7577-7580.

(48) Bian, J.; Ren, J.; Li, Y.; Wang, J.; Xu, X.; Feng, Y.; Tang, H.; Wang, Y.; Li, Z. Discovery of Wogonin-based PROTACs against CDK9 and capable of achieving antitumor activity. *Bioorg. Chem.* **2018**, *81*, 373-381.

(49) Zhao, Q.; Lan, T.; Su, S.; Rao, Y. Induction of apoptosis in MDA-MB-231 breast cancer cells by a PARP1-targeting PROTAC small molecule. *Chem. Comm.* **2019**, *55*, 369-372.

(50) Wang, S.; Han, L.; Han, J.; Li, P.; Ding, Q.; Zhang, Q.-J.; Liu, Z.-P.; Chen, C.; Yu, Y. Uncoupling of PARP1 trapping and inhibition using selective PARP1 degradation. *Nat. Chem. Biol.* **2019**, *15*, 1223-1231.

(51) Dawicki-McKenna, J. M.; Langelier, M. F.; DeNizio, J. E.; Riccio, A. A.; Cao, C. D.; Karch, K. R.; McCauley, M.; Steffen, J. D.; Black, B. E.; Pascal, J. M. PARP-1 activation requires local unfolding of an autoinhibitory domain. *Mol. Cell* **2015**, *60*, 755-768.

(52) Gadd, M. S.; Testa, A.; Lucas, X.; Chan, K. H.; Chen, W.; Lamont, D. J.; Zengerle, M.; Ciulli, A. Structural basis of PROTAC cooperative recognition for selective protein degradation. *Nat. Chem. Biol.*

2017, *13*, 514-521.

(53) Li, Y.; Yang, J.; Aguilar, A.; McEachern, D.; Przybranowski, S.; Liu, L.; Yang, C.-Y.; Wang, M.; Han, X.; Wang, S. Discovery of MD-224 as a first-in-class, highly potent, and efficacious proteolysis targeting chimera murine double minute 2 degrader capable of achieving complete and durable tumor regression. *J. Med. Chem.* **2018**, *62*, 448-466.

(54) Tinworth, C. P.; Lithgow, H.; Churcher, I. Small molecule-mediated protein knockdown as a new approach to drug discovery. *Med. Chem. Commun.* **2016**, *7*, 2206-2216.

(55) Toure, M.; Crews, C. M. Small‐molecule PROTACS: new approaches to protein degradation. *Angew. Chem., Int. Ed.* **2016**, *55*, 1966-1973.

(56) He, J. X.; Wang, M.; Huan, X. J.; Chen, C. H.; Song, S. S.; Wang, Y. Q.; Liao, X. M.; Tan, C.; He, Q.; Tong, L. J.; Wang, Y. T.; Li, X. H.; Su, Y.; Shen, Y. Y.; Sun, Y. M.; Yang, X. Y.; Chen, Y.; Gao, Z. W.; Chen, X. Y.; Xiong, B.; Lu, X. L.; Ding, J.; Yang, C. H.; Miao, Z. H. Novel PARP1/2 inhibitor mefuparib hydrochloride elicits potent in vitro and in vivo anticancer activity, characteristic of high tissue distribution. *Oncotarget* **2017**, *8*, 4156-4168.

(57) Redon, C. E.; Nakamura, A. J.; Zhang, Y. W.; Ji, J. J.; Bonner, W. M.; Kinders, R. J.; Parchment, R. E.; Doroshow, J. H.; Pommier, Y. Histone γH2AX and poly(ADP-ribose) as clinical pharmacodynamic biomarkers. *Clin. Cancer Res.* **2010**, *16*, 4532-4542.

(58) Papeo, G.; Posteri, H.; Borghi, D.; Busel, A. A.; Caprera, F.; Casale, E.; Ciomei, M.; Cirla, A.; Corti, E.; D'Anello, M.; Fasolini, M.; Forte, B.; Galvani, A.; Isacchi, A.; Khvat, A.; Krasavin, M. Y.; Lupi, R.; Orsini, P.; Perego, R.; Pesenti, E.; Pezzetta, D.; Rainoldi, S.; Riccardi-Sirtori, F.; Scolaro, A.; Sola, F.; Zuccotto, F.; Felder, E. R.; Donati, D.; Montagnoli, A. Discovery of 2-[1-(4,4-

difluorocyclohexyl)piperidin-4-yl]-6-fluoro-3-oxo-2,3-dihydro-1*H*-isoind ole-4-carboxamide (NMS-P118): a potent, orally available, and highly selective PARP-1 inhibitor for cancer therapy. *J. Med. Chem.* **2015**, *58*, 6875-6898.

Table of Contents graphic